# Study on properties of Praseodymium doped $NiO_x$ thin film as hole transport layer for perovskite solar cell


**By**

**Muhammad Tahir**

**Reg # 00000276956**

**Session 2018-20**

**Supervised by**

**Dr. Sehar Shakir**

**U.S.– Pakistan Center for Advanced Studies in Energy (USPCAS-E)**

**National University of Sciences and Technology (NUST)**

**H-12, Islamabad 44000, Pakistan**


**March 2022**

# Study on properties of Praseodymium doped $NiO_x$ thin film as hole transport layer for perovskite solar cell


**By**

**Muhammad Tahir**

**Reg # 00000276956**

**Session 2018-20**

**Supervised by**

**Dr. Sehar Shakir**

**A Thesis Submitted to U.S.-Pakistan Center for Advanced Studies in Energy**

**partial fulfillment of the requirements for the degree of**

**MASTER of SCIENCE in**

**THERMAL ENERGY ENGINEERING**

**U.S.– Pakistan Center for Advanced Studies in Energy (USPCAS-E)**

**National University of Sciences and Technology (NUST)**

**H-12, Islamabad 44000, Pakistan**

**March 2022**

## THESIS ACCEPTANCE CERTIFICATE

Certified that final copy of MS/MPhil thesis written by **Mr. Muhammad Tahir** (Registration No. **00000276956** ), of U.S.-Pakistan Center for Advanced Studies in Energy has been vetted by undersigned, found complete in all respects as per NUST Statues/Regulations, is within the similarity indices limit and is accepted as partial fulfillment for the award of MS/MPhil degree. It is further certified that necessary amendments as pointed out by GEC members of the scholar have also been incorporated in the said thesis.

Signature: _____

Supervisor: Dr. Sehar Shakir

Date: _____

Signature: _____

HOD-TEE: Dr. Majid Ali

Date: _____

Signature: _____

Principal: Prof. Dr. Adeel Waqas

Date: _____

# Certificate

This is to certify that work in this thesis has been carried out by **Mr. Muhammad Tahir** and completed under my supervision in Advanced Energy Material Lab laboratory, US-Pakistan Center for Advanced Studies in Energy (USPCAS-E), National University of Sciences and Technology, H-12, Islamabad, Pakistan.

Supervisor: _____

Dr. Sehar Shakir
USPCAS-E
NUST, Islamabad

GEC member 1: _____

Dr. Asif Hussain Khoja
USPCAS-E
NUST, Islamabad

GEC member 2: _____

Dr. Mustafa Anwar
USPCAS-E
NUST, Islamabad

GEC member 3: _____

Dr. Sarah Farrukh
SCME
NUST, Islamabad

HOD-TEE: _____

Dr. Majid Ali
USPCAS-E
NUST, Islamabad

Dean/Principal: _____

Prof. Dr. Adeel Waqas
USPCAS-E
NUST, Islamabad

# DEDICATION

This thesis is dedicated to my loving Parents

# Acknowledgment

First and foremost, all praise to **Allah Almighty**, The Most Beneficent, The Most Merciful, who gave me strength to achieve this goal. Second i want to give my genuine gratitude to my supervisor **Dr. Sehar Shakir** for her selfless guidance, tremendous support, and sharing a wealth of knowledge during my research work. I really appreciate her valuable critiques, comments, and suggestion during the thesis write-up. I believe that this thesis write-up would not have been possible to complete without her.

I also want to thank my graduate examination committee (GEC) members, Dr. Asif Hussain Khoja, Dr. Mustafa Anwar, and Dr. Sarah Farrukh who honored my committee presence and for having a major contribution in improving this thesis work.

I appreciate the support of faculty and lab engineers at USPCAS-E for all things that facilitated the research work and assistance every step of the way. I also indebt my lab fellows for their continuous help during the research.

Finally, and most importantly, I must express my very profound gratitude to my family who encouraged and facilitated me at every phase of my personal and academic life.

Thank You

Muhammad Tahir

# Abstract

Hybrid organic/inorganic Perovskite Solar Cells (PSCs) have acquired tremendous consideration due to their skyrocketing solar to power conversion efficiency from 3.9% to 29% has been achieved in just one decade, with efficient photovoltaic, electrical properties and simple manufacturing process. These properties make most promising photovoltaic technologies. However, there are numerous challenges in their development process, including the need for enhanced PCE, low stability, and toxicity. In planar p-i-n structure PSC, light harvesting layer (Absorber layer) is sandwiched between electron transport layer (ETL) and hole transport layer (HTL). Performance of PSCs is heavily affected by these interfaces between the layers. In our research work, to obtain undoped $NiO_x$ and Pr-doped $NiO_x$ thin film initially, $NiO_x$ and Pr-doped $NiO_x$ sols were prepared by sol-gel method. The concentration of Praseodymium ion (Pr-ions) was varied from (0 to 6 mol% ) subsequently, sols were spun on fluorine doped tin oxide (FTO) substrate and employed as a hole transport layer for PSC and further thin film was characterized by XRD, SEM/EDX, AFM, UV-Vis, Hall effect, contact angle, and IV-curve. The formation of cubical structure of $NiO_x$ and Pr-doped $NiO_x$ thin film were identified by X-ray diffraction (XRD) having crystallite size range between 28 nm to 12 nm and elemental composition of thin film were confirmed by Energy Dispersive X-Ray Analysis (EDX). Homogenous, uniform and crack free structure of thin film were confirmed by Scanning electron microscope and atomic force microscope (AFM). UV-Vis spectroscopy (UV-Vis) were used to determine the transmittance, absorbance, and band gap of sample. Electrical property of $NiO_x$ and Pr-doped $NiO_x$ thin film were calculated by hall effect measurement system (HMS). The Current density-voltage (J-V) curves of the cell revealed the performance of the device is remarkably improved when employing 4% Pr-doped $NiO_x$ HTL based PSC has shown that 9.23% PCE, resulting in 33.57% better improvement in PCE as compared to a device utilizing undoped $NiO_x$ based HTL.



**Keywords** *Perovskite solar cell, HTL, Praseodymium doping, solar cell, sol-gel*

# Table of contents

# List of Figures

# List of Tables

# List of Publication

1. Muhammad Tahir, Hafiz Abd-Ur-Rehman, Asif Hussain Khoja, Mustafa Anwar, Adil Mansoor, Faisal Abbas, Sehar Shakir. “Praseodymium doped Nickel oxide as Hole Transport Layer for efficient Planar Perovskite Solar cell.” *Journal of Alloys and Compound.* Submitted: 02 March 2022. Under Review: 09 March 2022.

# Abbreviations

| | |
|---|---|
| PSCs | Perovskite Solar Cells |
| HTL | Hole transport layer |
| LUMO | Lowest unoccupied molecular orbital |
| HOMO | Highest occupied molecular orbital |
| ETL | Electron transport Layer |
| PSCs | Perovskite solar cells |
| TCO | Transparent conducting oxide |
| QDS | Quantum dot solar cell |
| NPs | Nanoparticles |
| MEA | Monoethanolamine |
| FTO | Fluorine doped tin-oxide |
| rpm | Revolution per minute |
| SEM | Scanning electron microscopy |
| AFM | Atomic force microscopy |
| UV-Vis | Ultra-violet visible spectroscopy |
| J-V | Current voltage density curve |
| HEM | Hall effect measurement |
| DMF | Dimethylformamide |
| IPA | Isopropyl alcohol |
| DSSC | Dye-Sensitized solar cell |
| PCE | Power conversion efficiency |
| FTO | Fluorine-doped tin oxide |
| Eg | Bandgap |
| DMSO | Dimethyl sulfoxide |
| FF | Fill factor |

# Chapter 1: Introduction

## 1.1 World energy generation and energy crisis

Energy consumption around the globe has been frequently rising due to growing population and industrial advancement and this energy requirement is mostly full filled by non-renewable fuel sources such as these coal, petroleum, and natural gas. Most of the fossil fuels resources have been declining rapidly. Furthermore, fossil fuels are not ecologically friendly, resulting in anthropogenic greenhouse gas (GHG) emissions during these processes. The burning of fossil fuels, which is currently providing 85% of global energy needs, has resulted in 56.6% of all GHG emissions, as well as rising levels of carbon dioxide ($CO_2$), nitrous oxide ($NO_x$), methane ($CH_4$), Chlorofluorocarbon (CFC) and Sulphur oxide ($SO_x$), which has a significant impact on global warming, abrupt climate change and malicious health effect on the human body such as respiratory disorder and skin related diseases. The rising rate of these gases causes the atmosphere trap more of sun's heat possibly causing the increase in temperature of the atmosphere, a phenomenon known as global warming [1, 2].

Global warming is increasing at a rate of 0.13 °C per decade, with predictions that the rate will increase to 0.5 °C in the next ten years [3]. These GHG emissions can be reduced in different ways from energy structure while providing energy services on a continuous basis. In the meantime, in 2017 the main contributors to power generation were coal, petroleum, and gas with a combined contribution of 73.5% followed by inexhaustible energy sources like solar, hydro, and biomass, etc. [4].

## 1.2 Alternative sources of energy

Nuclear energy is being seen in both developed and under-developing countries as a viable alternative resource like (Coal, Petroleum, and Natural gas, etc.). However due to its high capital and operating cost, hazard to the environment, technical dominance, and limited availability It is not easily available in many countries worldwide.

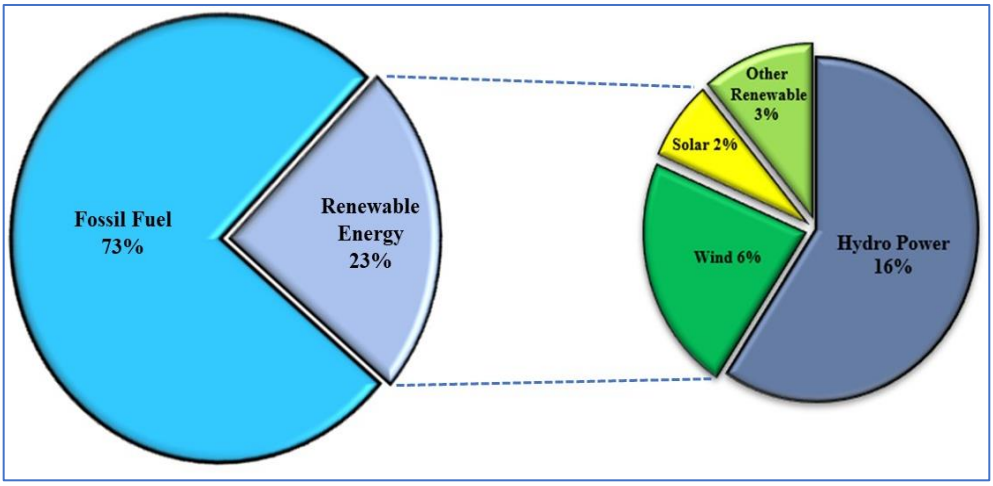


Figure 1-1 World energy generation of renewable and nonrenewable sources [4].

Scientists are attempting to harvest energy from various renewable sources to meet their energy demands while avoiding the use of fossil fuels. Renewable energy (RE) technologies are a clean and green source of energy that can meet energy demands of everyday life. Alternative energy sources such as wind, solar, hydro, biofuel, and geothermal energy can be used to meet current and future energy needs, without the emission of hazardous gases, resulting in a reduction of environmental impacts [5].

The graph in Fig 1.1 exhibits the share of electricity generation from wind, solar, geothermal, biomass, and other renewable sources during the last decade in the world. In 2010, the world's dependence on renewable sources mostly (wind and solar) was generated around 110-Terawatt hour (TWh) green energy furthermore, 358-Terawatt hour (TWh) was added in green energy in 2020. These two-renewable energies (wind and solar) sources accounted for nearly all global electricity generation. Meanwhile, because of the relentless escalation of renewable energy, electricity produced by the solar, hydroelectric power plant, and the wind are relatively safe for the environment. According to the analysis, worldwide wind and solar power capacity will increase by 238 GW in 2020, more than five times the UK's total renewable energy capacity [6]

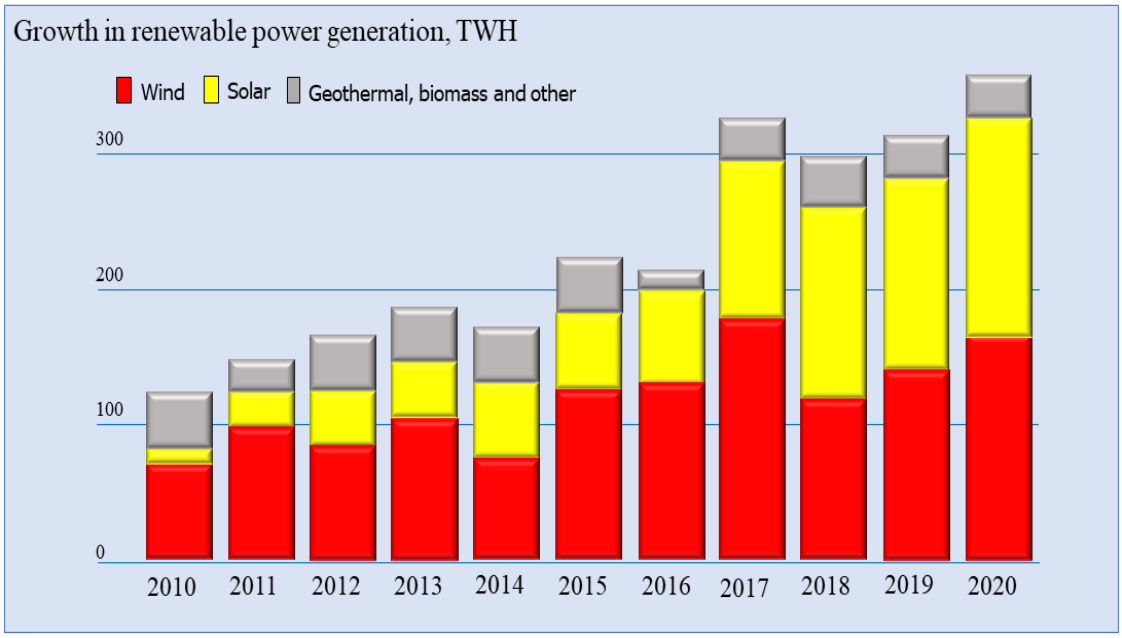


Figure 1-2 Share of wind-solar geothermal biomass and other energy growth in renewable power generation in the world 2020 [6].

All renewable sources such as biomass, geothermal, wind, biofuel, solar thermal energy, and PV-technology, etc. should be encouraged to meet current and future energy demand as a green energy source. Among them solar energy is a promising renewable energy candidate should be efficient, cost-effective, climate and eco-friendly.

## 1.3 Solar energy outlook in Pakistan

Pakistan is reclined on the sunny belt and it has much potential for solar energy so that's why promoting renewable solar energy to get the advantage of the sunny belt. On average, it receives about 1 KW of solar energy per square meter of an area of land for 6 to 7 hours per day. The number of sunshine hours per year is nearly 3000-3300 [7]. The weather is most favorable for the utilization of solar energy. In the 2015 solar assessment survey conducted by the World Bank, it was determined that Pakistan receives 2000 $kWh/m^2$ of AM 1.5 solar irradiation every year. Another study conducted by the National Renewable Energy Laboratory in collaboration with several other organizations found that over 80% of the country receives 6 $kWh/m^2$/day of direct normal solar irradiation.

Northern parts of Baluchistan receive the highest values which reach a maximum of 2700 $kWh/m^2$. The weather in Pakistan is also ideal for solar energy generation because there

are large plains that are unaffected by cloud cover, aerosol content, irradiance diffusion, or air pollution [8, 9].

## 1.4 Solar energy technologies

The sunlight energy coming from the sun is a promising candidate. Solar energy is being converted into the electrical energy by a different technological aspect such as concentrating solar thermal power (CSP) solar photovoltaic (PV) and solar thermal energy (STE) Each of these transform's sunlight into an energy form.

### 1.4.1 Solar thermal energy

STE is a well-known one of the most reliable technology for harnessing solar energy to generate thermal energy for use in commercial sectors, and industry for heating and cooling a purpose. The heat from the sun can be collected and transported in a medium, and that stored thermal energy can then be further used for such purposes as heating and cooling a home, hot water heating, cooking food, and power generation [10].

### 1.4.2 Concentrating Solar Power

CSP is one of the valid technologies which generates electricity by using mirrors configuration to concentrate (focus) the sun's light energy in a single focal point. This concentrated energy is converted into high-temperature heat then used to heat up a fluid, produce steam, and drive turbines to produce electrical power. it is mostly used for industrial purposes because of large-scale power plants [11].

### 1.4.3 Solar photovoltaic

Sun based energy is an easily available renewable resource. It does not need to be imported from other regions of the country or across the world. It is widely accessible in all parts of the world and is available 24 hours a day. Unlike some other energy sources, solar energy will never run out.

Solar photovoltaics energy or PV is an elegant technology of direct conversion of sunlight into D.C. electric power, using a technology based on fundamental principle of "photovoltaic effect". When sunlight strikes a solar PV cell, the semiconductor releases electrons, resulting in an electric current. This phenomenon is exhibited in semiconductor materials [12].

## 1.5 Working of Solar cell

The solar cell also knowns as the PV cell is an optoelectronic device that converts optical energy into electric power. Incident sunlight consists of well-defined tiny energy particles, which are so-called photons. When a PV cell is exposed to sunlight, many photons are absorbed or pass right through depending on the optical properties of devices such as anti-reflecting coating thickness, absorber surface, metal surface, and surface area [13]. When sun light is captured by a p-type layer of a cell at moment electrons are freely moved from negative semiconductor material. Due to the manufacturing process of the positive layer, these freed electrons move to the N-type layer generating a potential difference, similar to a household battery. Electrons flow through the circuit and creating electricity, when two layers are connected to a load. An antireflecting coating for maximum absorption of sunlight and front metal contacts for collection of generated electrons as displayed in Fig 1.3 [14].

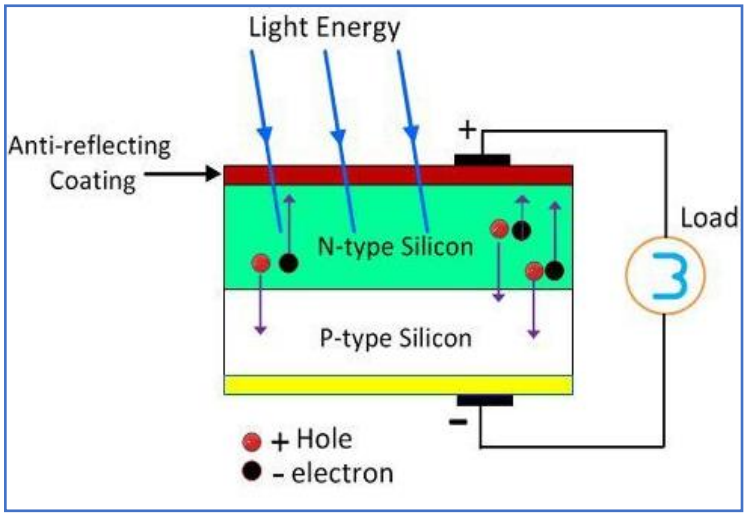


Figure 1-3 Photovoltaic Cell [15].

## 1.6 Types of Photovoltaic Solar cell

The classification of Solar cells is further categorized based on their types of materials that are used. on their generation and type of material. Categorically photovoltaic cells are divided into three generations which accounts for their cell structure, material type, and type of absorber material which initiates the conversion of photon into electricity [16].

There are three generations of solar cells, and all are discussed briefly in this section.

### 1.6.1 First generation solar cell

First generation solar technology is based on crystalline silicon semiconducting material. This is the earliest and most primitive technology. These are crystal base solar cells those are consisting of poly crystalline or single crystal solar cell. Silicon was the only known material used to make that possible solar cell does not contain silicon It is doped with either Phosphorus or Boron to make it a p-type and n-type material. Because of its higher efficiencies of up to 25%, it is one of the most popular technologies. These are solar cells associated with high material consumption, high processing cost, huge loss of material, and its losses potential in the future due to relatively low efficient [17].

Figure 1-4 Multi-Crystalline Silicon Solar Cell panel [18].

### 1.6.2 Second generation solar cell

Second generation of Solar Cells are based on thin-film solar cells subsequently crystal-based Silicon Solar Cells (poly crystalline or single crystal solar cell). The thin layer of Semi-conductor material is used to create the thin film of a solar cell. This would be generation preferred the in comparison to the first due to low-cost fewer material usages and lower efficiency than 1$^{st}$ generation solar cell. These thin-film solar cells are produced by various deposition techniques like CVD and PVD. The materials used include CdTe, CIGS, CZTS, and amorphous silicon [19].

Second-generation solar cell is less expensive and can be manufactured easily in less time as compared to first generation solar cell. Furthermore, the benefit of these technologies

is lowered module masses. The drawbacks of second generation are lower efficiency as compared with first generation cells and instability of amorphous silicon.

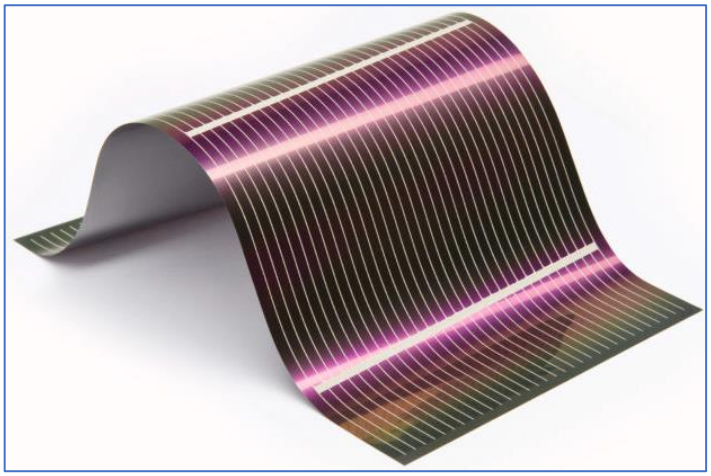

Figure 1-5 Thin-Film Solar Cells [20].

### 1.6.3 Third generation solar cell

Researchers have developed a new generation of solar cells to achieve remarkable efficiency while keeping costs low, to achieve higher efficiency. As compared with conventional PN- Junction solar cell, third generation of solar cells has entirely distinct structure and operation mechanism of cell. New emerging semiconductor materials and PV technologies are used in third-generation solar cells such as organic OSC, QDSC, DSSC, and PSC, Due to their minimum cost of manufacture and high efficiency, these solar cells are a research focus for researchers. It is based on solution-processable therefore these kinds of solar cells are fabricated by the chemical and physical route. A typical DSSC device includes a semiconductor photoanode, usually titanium dioxide ($TiO_2$), a counter electrode, and an electrolyte. Under light illumination, the dye sensitizer generates photoelectrons, which are injected into the $TiO_2$ conduction band [21]. To reach the counter electrode, electrons flow out through the back contact and external load. Organic-based photovoltaic (OPV) and the dye-sensitized system have modest efficiencies, with a PCE of 8.3% [22]. Now a day PSCs which are also part of the organic

structure are under the research phase and the highest lab efficiency value 25% is achieved but it holds a little share of the market [23].

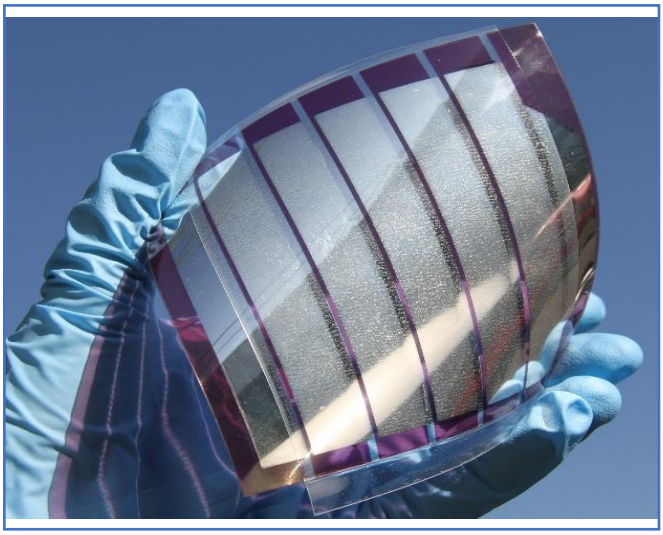

Figure 1-6 Organic solar cell [24].

## 1.7 Perovskite solar cell

A long-standing solar cell with reported efficiency is 9.3% was made in 2009 by Miyasaka and coworkers using photoactive material in place of liquid electrolyte introducing a whole new dimension of solar cells termed as PSCs, which is included in the third-generation solar cell [25]. Organic-inorganic hybrid methylammonium lead halide ($CH_3NH_3PbI_3$) has drawn a huge amount of attention from academics and industry research within the last decade due to their low production cost, phenomenal optoelectronic properties, high carrier mobility, high absorption coefficients, and high-power conversion efficiency [26]. With the development of PSC devices, the researcher discovered several device structures including the mesoporous structure and planar structure which can be divided into the regular n-i-p structure and inverted p-i-n structure. The solar cell p-i-n configuration is consisting of transparent conducting oxide followed by a HTL, perovskite absorbing layer and ETL, and silver back contacts [27, 28]. In new research, this modification is just as important as the basic organic materials used in HTL. As a result, using nanotechnology, this study was conducted on a single component of HTLs.

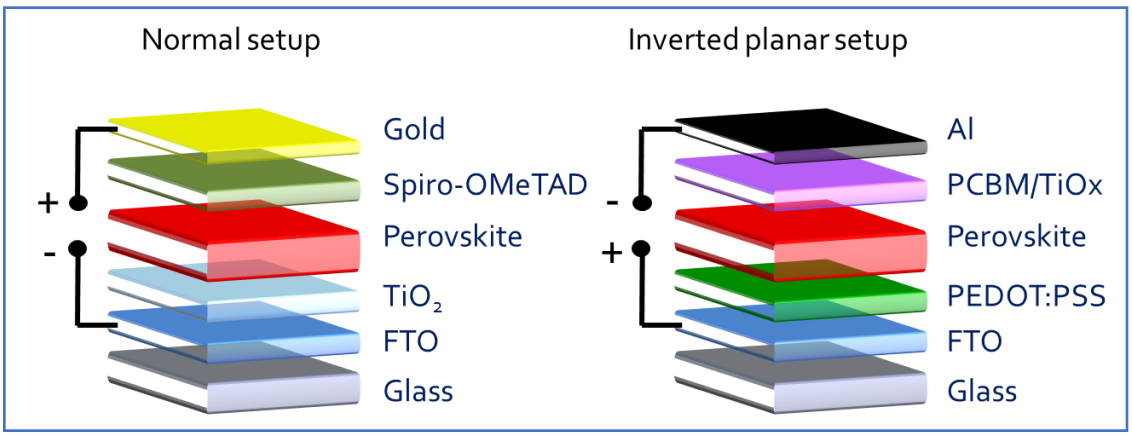


Figure 1-7 Stack structure for standard and inverted perovskite solar cell [29].

## 1.8 Problem Statement

HTL plays a significant role to improve the performance and enhance efficiency PSCs. Moreover, it can also improve the rate of charge carrier extraction and minimize the energy losses of photogenerated carriers in the absorber layer. To date, the most popular HTL is poly(3,4-ethylenedioxythiophene): polystyrene sulfonate PEDOT:PSS [30] was broadly employed as HTL in PSC however it is not ideal because of its acidic and hygroscopic nature tendency to absorb the water-induced decayed interface between the FTO and PEDOT:PSS and inability to block the electron. Alternatively, different doping P-type inorganic-material $Cu_2O$ [31], CuSCN [32], $V_2O_5$ [33], and $NiO_x$ [34] among the above the HTL material $NiO_x$ is one of the most favorable p-type inorganic semiconductor materials for HTL in planar PSCs due to its better chemical stability, large bandgap ( >3.4), hole extraction and electron blocking and deep valence band (5.4 eV) [35]. But $NiO_x$ possess the unsatisfactory electrical property such as low conductivity which could degrade the stability and performance of PSC so to overcome these key challenges metal doping have been reported to be a feasible path to minimize surface trap density and enhance the conductivity.

## 1.9 Aim of Research

At the start of this study, there were some gaps between $NiO_x$ based inverted PSCs device and mesoporous regular device particularly the much diminish efficiency and poor film quality, in order to facilitate the development of inverted planar structure PSCs based

$NiO_x$ device. This research is aimed to synthesize the pure $NiO_x$, and Praseodymium doped nickel oxide (Pr-$NiO_x$) with different concentrations of praseodymium 2, 4, and 6 mol% as a dopant and this was achieved via using sol-gel method. Subsequently, the perovskite absorber layer, ETL, and contacts were attached to a device. The sample-based various concentration of Pr was characterized by morphological and structural scans with XRD, SEM/EDS, AFM. Thermal and optoelectronic studies were also employed to study check absorptionand thermal stability parameters. Hall Effect measurement and current density-voltage (J-V) measurements were used to detect electrical characteristics

## 1.10 Challenges and limitation of Research

### Challenges of research

Following are few challenges in their development process of PSCs

- Fast degradation under humid condition.
- Low stability.
- Material toxicity.

### Limitation of research

- There are few major limitations in their development of PSCs on commercialization such as sever light intensities, high temperature, moisture, and frequently weather changes.
- Glove box is necessary for fabrication of PSCs device.

## 1.11 Thesis Objective

The objectives of this study are

- To synthesis $NiO_x$, Pr doped $NiO_x$ sol, and synthesis Pr-dopped $NiO_x$ thin film as HTL for inverted (p-i-n) configuration of PSC structure by Sol-gel method.
- To study morphology, optoelectronic and electrochemical properties of Pr-dopped $NiO_x$ HTL for PSC.
- To compare the device efficiency of undoped and Pr-doped $NiO_x$ of PSCs.

## 1.12 Scope of thesis

There are three interacting stages are followed in this research work consisting of material synthesis, characterization, and IV performance of PSCs. In the first stage synthesis of undoped $NiO_x$ with different concentrations (0,2,4 and 6 mol%) Pr-doped $NiO_x$ thin film as HTL based Perovskite solar cell by solution process method and deposited on FTO glass substrate by mean of employing spin-coated method. In the second stage, the thickness of thin films was measured approximately 34 nm by optical profilometry, and device active area is specified by approximately 1.2 $cm^2$. In the last stage, these thin films were used as HTL in PSCs to obtain the high efficiency and good stability of cells.

## 1.13 Thesis outline

**Chapter 01** provides a brief introduction to energy generation and crises along with alternative sources of renewable energy like wind, solar, geothermal, biomass, and others, followed by different solar energy technologies such as solar thermal energy, concentrating solar power, and photovoltaic solar cell, in addition including with different generation of the solar cell.

**Chapter 02** summarizes the literature review conducted on PSCs and briefly discussed structure and formula of perovskite material and origin of PSCs, followed by the device configuration, working of perovskite solar cell along with preparation of different type of layers such as ETL, HTL and light-absorbing layer.

**Chapter 03** deposition techniques are discussed like sputtering, chemical spray pyrolysis method, and pulsed laser deposition method. The primary focus of this chapter is the synthesis of $NiO_x$ and Pr-doped $NiO_x$ sols via the sol-gel technique and deposited onto FTO glass. The experimental process flow diagram starting until the end of deposition is also presented. A brief description of different characterization techniques such as structural, morphological, and electrical properties employed in this research work.

**Chapter 04** represent the result and discussion of this research work. $NiO_x$ and Pr-doped $NiO_x$ thin film are studied in this chapter. While the properties of the thin film are included in the thickness of the film, structural, morphological, and electrical properties are examined in detail.

**Chapter 05** discusses the conclusions of this study along with some recommendations for future work.

## Summary

This chapter provides firstly brief an overview of energy generations and its crises across the globe, discuss the impacts of fossil fuel on the environment, focusing the importance of the alternative sources of renewable energy, and solar potential of Pakistan reclined on the sunny belt is also addressed under radiation outlook in Pakistan along with briefly discuss the solar energy-based technologies such as STE, CSP, and photovoltaic. After that basic structure and working principle of the solar cell are explained. discussing the mainly three generations of the photovoltaic solar cell. The first generation of solar cell is used silicon-based wafer technology, while the second-generation photovoltaic solar cell is employed compounds of group III-V, halides, and thin film-based technology. Second-generation solar cell is less expensive and can be manufactured easily in less time as compared to the first generation. third-generation solar cell deal with are various nano-material-based solar cell technology such as organic solar cells, DSSCs, and PSCs are among the third generation of the photovoltaic solar cell. The efficiency of these type of solar cell has achieved almost 30%. The main objective of this research is to Pr-doped $NiO_x$ as a HTL for efficient planar PSC.

## References


1. K. S. Ottmar Edenhofer et al., “IPCC Special Report on Renewable Energy Sources and climate change Mitigation Summary for Policy maker, ” no. May 2011, pp. 5-8.
2. O. Edenhofer, R.P. et al., “Renewable energy sources and climate change mitigation: Special report of the intergovernmental panel on climate change”. Cambridge University Press. (2011).
3. A.H. khan, “A Primer on Pakistan’s Energy Mix - Daily Pakistan Global,” daily pakistan global, (2018) 3.
4. Baloch, M.H., et al., , “Hybrid energy sources status of Pakistan: An optimal technical proposal to solve the power crises issues. Energy Strategy Reviews, 2019”. 24: p. 132-153.
5. "Types of Alternative Energy Sources You Can Use Today." | Inspire [Online]. Available from: https://www.inspirecleanenergy.com/blog/clean-energy-101/types-of-alternative-energy [Accessed: 10-Oct-2019].
6. Ambrose., J. "Global wind and solar power capacity grew at record rate in 2020" | Energy industry [Online]. Available from: https://www.theguardian.com/business/2021/jul/08/bp-global-wind-and-solar-power-capacity-grew-at-record-rate-in-2020 [Accessed: 12-Oct-2019].
7. Ulfat, I., et al., , Estimation of Solar Energy Potential for Islamabad, Pakistan. Energy Procedia, 2012. 18: p. 1496-1500.
8. Tahir, Z.R. et al., Surface measured solar radiation data and solar energy resource assessment of Pakistan: A review. Renewable and Sustainable Energy Reviews, 2018. 81: p. 2839-2861.
9. S. Stökler, C.S., et al., “Solar resource assessment study for Pakistan, ” Renewable and Sustainable Energy Reviews, vol. 58. 2016, pp. 1184–1188,
10. “Solar heating and cooling technologies.” | EPA [Online]. Available from: https://www.epa.gov/rhc/solar-heating-and-cooling-technologies [Accessed: 12-Oct-2019].

11. “Concentrating Solar- Thermal Power Basics.” | solar energy technology office [Online]. . Available from: https://www.energy.gov/eere/solar/concentrating-solar-thermal-power-basics [Accessed: 12-Oct-2019].
12. “Solar photovoltaic technology basics.” | NREL Transforming Energy [Online]. Available from: https://www.nrel.gov/research/re-photovoltaics.html [Accessed: 12-Oct-2019].
13. “The science of solar explained.” | [Online]. Available from: https://solect.com/the-science-of-solar-how-solar-panels-work/ [Accessed: 12-Oct-2019].
14. Corkish, R., Solar Cells, in Encyclopedia of Energy, C.J. Cleveland, Editor. 2004,. p. 545-557.
15. "Circuit globe" [Online]. Available from: https://circuitglobe.com/photoelectric-transducer.html [Accessed: 12-Oct-2019].
16. Kibria, M.T., et al. , A Review: Comparative studies on different generation solar cells technology. in Proc. of 5th International Conference on Environmental Aspects of Bangladesh. 2014.
17. Badawy, W.A., A review on solar cells from Si-single crystals to porous materials and quantum dots. Journal of Advanced Research, 2015. 6(2): p. 123-132.
18. “PHYS ORG” [Online]. Available from: https://phys.org/news/2015-06-large-area-industrial-crystalline-silicon.html [Accessed: 12-Oct-2019].
19. “2nd- genration soalr cell technologies.” | Ossila [Online]. Available from: https://www.ossila.com/pages/organic-photovoltaics-vs-2nd-gen-solar-cell-tech [Accessed: 15-Oct-2019].
20. “Scot Amyx” [Online]. Available from: https://scottamyx.com/2019/05/21/second-generation-thin-film-solar-cells/ [Accessed: 12-Oct-2019].
21. B. E. Hardin, et al., “The renaissance of dye-sensitized solar cell " Nature Photon **6,** (2012) p. 162–169
22. “Organic solar cell efficiency record set by konarka.” | Energy Matter [Online]. Available from: https://www.energymatters.com.au/renewable-news/em1213/ [Accessed: 15-Oct-2019].

23. Kim, Min, et al., Impact of strain relaxation on performance of α-formamidinium lead iodide perovskite solar cells. Science 370(6512), S. I. (2020). ,108–112.
24. " The solar institute" [Online]. Available from: https://thesolarinstitute.org/solar-tech/ [Accessed: 12-Oct-2019].
25. Kim, H.-S., et al., Organolead Halide Perovskite: New Horizons in Solar Cell Research. The Journal of Physical Chemistry C, 2014. 118(11): p. 5615-5625.
26. Pitchaiya, S., et al., , A review on the classification of organic/inorganic/carbonaceous hole transporting materials for perovskite solar cell application. Arabian Journal of Chemistry, 2020. 13(1): p. 2526-2557.
27. Mahapatra, A., et al., , A review of aspects of additive engineering in perovskite solar cells. Journal of Materials Chemistry A, 2020. 8(1): p. 27-54.
28. Mali, S.S.a.C.K.H., p-i-n/n-i-p type planar hybrid structure of highly efficient perovskite solar cells towards improved air stability: synthetic strategies and the role of p-type hole transport layer (HTL) and n-type electron transport layer (ETL) metal oxides. Nanoscale, 2016. 8(20): p. 10528-10540.
29. " ZSW" [Online]. Available from: https://www.zsw-bw.de/en/research/photovoltaics/topics/perovskite-solar-cells.html [Accessed: 12-Oct-2019].
30. Jørgensen, M., et al., Stability/degradation of polymer solar cells. Solar Energy Materials and Solar Cells, 2008. **92**: p. 686-714.
31. Zuo, C. et al., Solution-Processed Cu2O and CuO as Hole Transport Materials for Efficient Perovskite Solar Cells. Small, 2015. **11**(41): p. 5528-5532.
32. Jin, I.S., et al., Molecular doping of CuSCN for hole transporting layers in inverted-type planar perovskite solar cells. Inorganic Chemistry Frontiers, 2019. **6**(8): p. 2158-2166.
33. Peng, H., et al., Solution processed inorganic V2Ox as interfacial function materials for inverted planar-heterojunction perovskite solar cells with enhanced efficiency. 2016. **9**: p. 2960-2971.
34. Chen, W., et al., Cesium Doped NiOx as an Efficient Hole Extraction Layer for Inverted Planar Perovskite Solar Cells. Advanced Energy Materials, 2017. **7**(19): p. 1700722.

35. Xu, L., et al., Inverted perovskite solar cells employing doped NiO hole transport layers: A review. Nano Energy, 2019. **63**: p. 103860.

# Chapter 2: Literature Review

## 2.1 General introduction of Perovskite solar cell

Gustav Rose discovered the Calcium Titanate ($CaTiO_3$) mineral in the Ural Mountains of Russia in 1839 and named it "Perovskite" after a Russian mineralogist named "L. A. Perovski." (1792–1856)" [1]. Perovskites are a family of materials described by the chemical formula $ABX_3$, where A, B can be cations and X can be an anion typically (oxygen, carbon, nitrogen or a halide) that bonds to both as shown in Figurer 2.1. Perovskites are usually categorized as halide perovskites ($ABX_3$) and metal oxide perovskite ($ABO_3$) [2]. Halide perovskites (X = F, Cl, Br, I) are used for solar cell applications. Perovskite can further classify organo-metal halide perovskites and alkali halide perovskites. For the photovoltaic utilization, the large cation A is usually the organic ion such as methylammonium ($CH_3NH_3$, MA) and formamidinium ($NH_2CH{=}NH_2$, FA) or a typical inorganic Cesium ion $Cs^+$, the smaller cation B is lead ion ($Pb^{2+}$) or the tin ion ($Sn^{2+}$), where the X is a halogen ion like $Br^-$, $I^-$ and $Cl^-$ or pseudohalogen ion like SCN [3].

Perovskite is likely considered to be a promising material for photoelectric devices, due to its attractive properties such as (long diffusion length, high absorption coefficient, low-temperature process, bandgap tunable, and low trap densities). Their superior optical and electrical properties make them take part in ideal candidates in solar cell light-emitting diode laser and photoelectrode [4].

The perfect crystal structure of perovskite ($MAPbI_3$) material allows optimal band gap of 1.55 eV which is most suitable for sun light absorption up to a wavelength of 800 nm. The perovskite containing halide group as anion have good optical, electrical, and magnetic properties due to its special crystal structure. Organic-inorganic hybrid methylammonium lead halide perovskites ($CH_3NH_3PbI_3$) have become a new attractive photovoltaics material due to their high-power conversion efficiencies, low cost, remarkable optical and electronic properties.

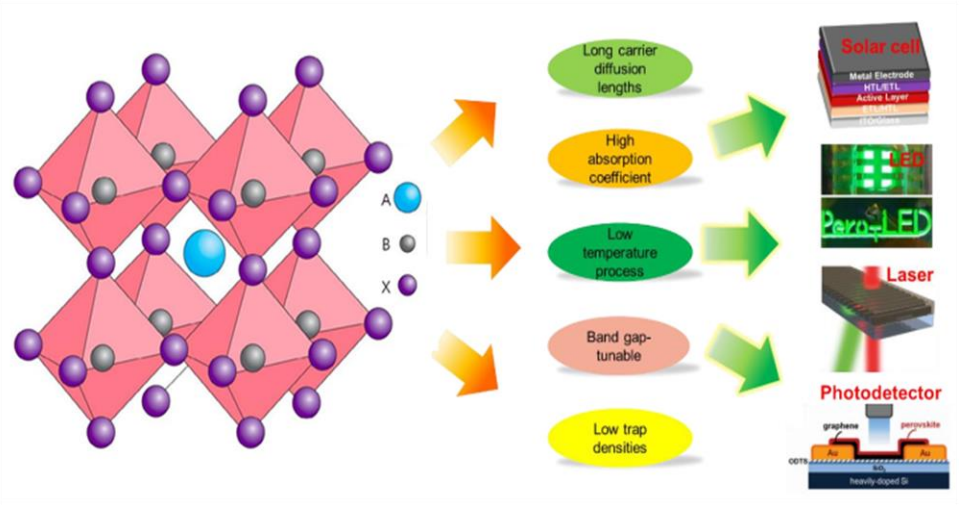


Figure 2-1 Crystal structure of Perovskite solar cell [5]

The key function of A cation is to fill the 12-fold cuboctahedral voids generated by corner connected octahedral BX6, that halide enrich $BX_6$ octahedral also enrich in -iv charge so monovalent cation A also neutralizes this charge. The size of A cation has crucial effect on octahedral structure integrity. The selection of A-site cation will be restricted by several criteria. The most important restriction is the size. The A cation must match into $BX_6$ cuboctahedral voids.

The Goldschmidt tolerance factor (t) is used to determine the structural stability of perovskite compounds.

$$t = \frac{r_A + r_X}{\sqrt{2}\,(r_A + r_X)}$$

Where $r_A$, $r_B$, and $r_x$ are the ionic radii of A, B, and X, respectively when t = 1 and it can be varied only in a restricted range. For most perovskites, it has been stated to be between 0.8 and 0.9 [6, 7]. Improper size ions lead to a distorted network and make a non-perovskite structure with t < 0.8. Distinguished advantages suitable for optoelectronics often vanish when switching to the non-perovskite structures.

These cells can be produced on variety of substrates like metal, polymeric and glass substrates. These cells can be made on flexible or robust substrates. They absorb and convert light from both sides of panels.

### 2.1.1 Origin of perovskite solar cell

In the initial work reported by Miyasaka, et al. were used perovskite materials as semiconductors in DSSC for the first time in 2009, using a $TiO_2$ electrode (anode) and an FTO/glass counter electrode (cathode), getting 3.8% efficient device with methylammonium lead iodide and 3.1% methylammonium lead bromide, which shown very bad stability performance.[8] after Miyasaka et al in 2012 Gratzel et al. Grätzel and Park's groups, followed by Miyasaka and co-workers in collaboration with Snaith's group, built PSC utilizing a TiO2 mesoporous layer (mp-TiO2) and replaced the DSSC's liquid electrolyte with a compact layer manufactured with spiro OMeTAD in 2012, which drastically enhanced stability of cell [9]. Latterly, the device structure was developed into solid-state which showed a significant improvement in device performance and stability.

## 2.2 Device Configuration

A typical PSC utilizes perovskite material which is sandwiched between an ETL on a transparent conducting oxide (TCO) glass and HTL, coated with a metal back contact electrode. PSCs divided into two basic cell configurations such as inverted planar (p-i-n) hybrid, and regular type planar n-i-p structure of PSC as depicted in Fig. 2.2 (a and b) depict the n-i-p and p-i-n structures of PSC, respectively. Fig. 2.2 (c and d) depicts the energy level diagrams of the n-i-p and p-i-n PSC, respectively.

For n-i-p structure PSCs are further categorized into two types planar and hetero-structure. PSC that demonstrated the original concept of the solid-state DSSC. Regular planar (n-i-p) and inverted planar (p-i-n) structures have been used to divide these types based on the type of HTL and ETL.

The breakthrough of the planar perovskite structure was obtained by using a dual source vapor deposition, providing dense and high-quality perovskite films that achieved 15.4% efficiency. Recently, the efficiency of the planar structure was pushed over 19% through interface engineering. The p-i-n structure is a derivative of the organic solar cell, and typically, numerous charge transport layers used in organic solar cells were successfully relocated into solid state PSCs.

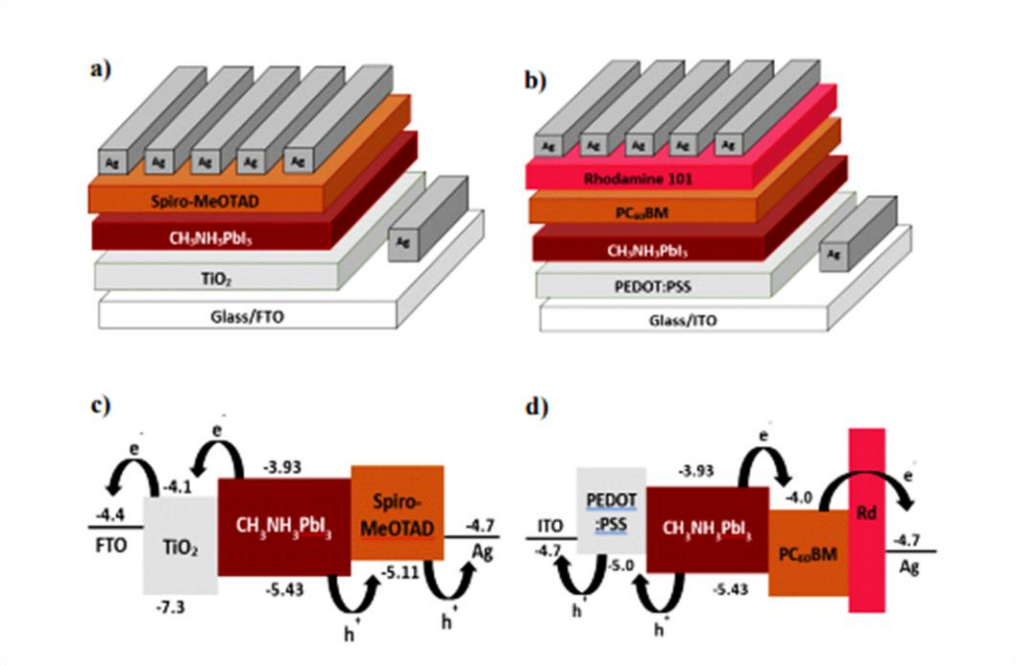


Figure 2-2 (a) Regular (n-i-p) (b) inverted (p-i-n) structures of perovskite solar cell and Energy level diagram (c) regular (d) ) inverted (p-i-n) PSC [3].

## 2.3 Device working principle

PSCs is a device that converts light sun-based energy into electrical energy by photovoltaic effect phenomena. In this cell light-harvesting material (Perovskite material) is used to capture the incident light and the electron is excited from the ground state i.e., HOMO of valance band to excited state LUMO of the conduction band.

When the sunlight reached perovskite material, the formation of excitons (electron-hole pair) may generate with respect to the bandgap and absorption coefficient of the material. These excitons can get diffused into the material, decreasing the number of excitons reaching the acceptor/donor junction. Thus, short diffusion lengths can reduce the solar cell efficiency [10] [11].

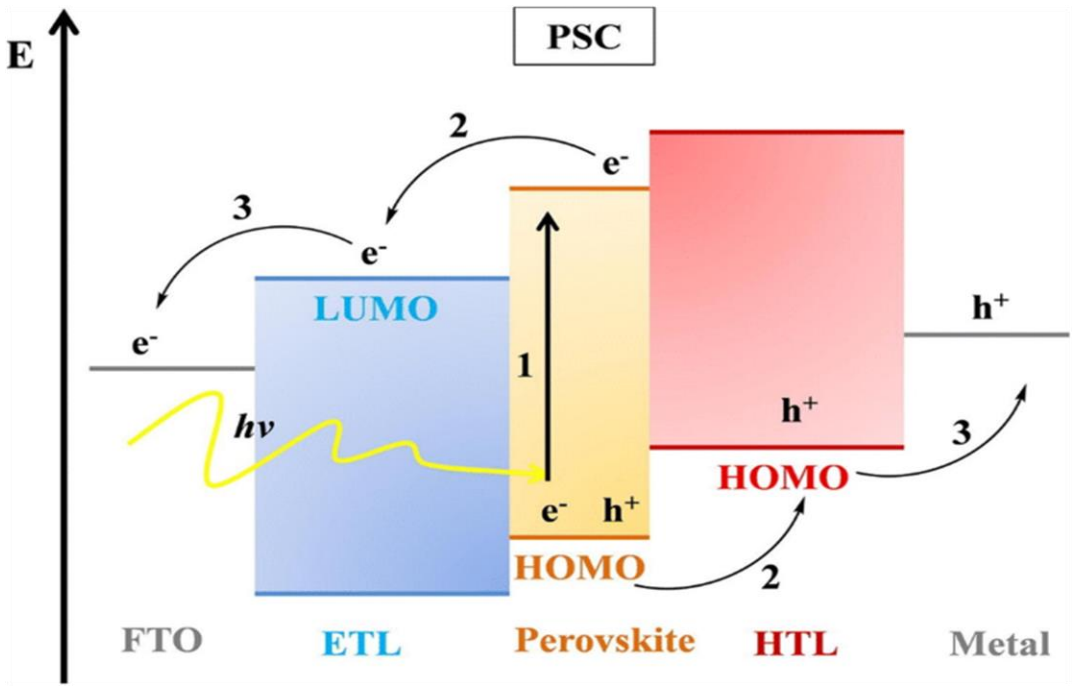


Figure 2-3 Schematic representation of the energy levels electron and hole transfer process [10].

The excitons are supposed to be broken, with electron and hole getting separated. It is hard to remove charges from each other. Hence, it may cause recombination, drifting the exciton to the ground state. Recombination can be a lethal hindrance to the efficiency of solar cells. After the separation, an electron from LUMO of conduction band jumps to conduction band of ETL while, an electron from HOMO of the HTL jumps to HOMO of valance band of the material.

## 2.4 Preparation of Perovskite solar cell

### 2.4.1 Electron transport layer

The ETL is used to extracts electron from light-harvesting materials. Three various types of ETLs are considered. In 1st type of ETL is n-type material which is usually used mesoporous $TiO_2$ in PSC. Its role is to inhibit electrons from being regained by HTL. The function of the second type of ETL is the same as the first. However, It's for PSCs with inverted structures. In most cases, a blocking layer is placed between this layer and metal back contact. This layer is generally created as a dense-thin film, according to

morphology. The third type of ETL is a bifunctional layer, which functions both as the ETL and blocking layer.

### 2.4.2 Hole transport layer

In a PSC, HTL is used to extract the hole from perovskite material and block the electron the quenching caused by the direct contact between perovskite and the metal electrode can be avoided when HTL is introduced. Different types of materials have been considered and used as HTLs consequently, including organic molecules such as (Such as Spiro-OMeTAD and PTAA) and inorganic material CuI [12], $Cu_2O$ [13], CuSCN [14], $CoO_x$, [15] $Cu_2BaSnS_4$, [16] and $NiO_x$ [17] have emerged for PSCs application because they have several advantages such as lower fabrication cost, higher stability, higher carrier mobility and better optical transparency in infrared (IR) and visible regions with higher work function.

#### 2.4.2.1 Nickel Oxide $NiO_x$

Among the many p-type inorganic compounds such as CuI, CuSCN, $CoO_x$, $Cu_2BaSnS_4$, etc. tested in inverted (p-i-n) structure, all devices based on $NiO_x$ HTL possess more than 20% PCE. Moreover, these photons to electron conversion efficiency are comparable with the highest PCE achieved in inverted PSCs. $NiO_x$ is the most favorable p-type inorganic semiconductor material for HTL in planar PSCs due to its better chemical stability, hole extraction, electron blocking, and large bandgap [18].

$NiO_x$ HTLs can be made easily using a variety of methods, including solution procedures, pulsed laser deposition, electrochemical deposition method, combustion methods, atomic layer deposition, and so on.

**Table 2-1** Summary of the different Organic based HTL PSCs devices

| S.No | HTL | FF | PCE (%) | Advantages | Dis-advantages | Ref |
|---|---|---|---|---|---|---|
| 01 | PEDOT:PSS | 0.61 | 7.05 | Good conductivity and optical transmittance. High work function | Hygroscopic nature and tendency to absorb water | [19] |
| 02 | Spiro-OmeTAD | 0.73 | 13.0 | ease of processing and good hole conductivity | High cost and complicated synthesis | [20] |
| 03 | PTAA | 0.76 | 16.2 | Thermally stable and soluble in a wide range of organic solvents, with high hole mobility. | High cost and multistep synthesis | [21] |

**Table 2-2** Summary of the different In-Organic based HTL PSCs devices

| S.No | HTL | FF | PCE (%) | Advantages | Dis-advantages | Ref |
|---|---|---|---|---|---|---|
| 01 | CuScn | 0.78 | 15.3 | It has a large bandgap, as well as outstanding optical and electrical properties. It has excellent environmental stability and prevents moisture from infiltrating the device. | No competitiveness which is deprived by its deposition complexity, as a large thickness (>1um) | [22] |
| 02 | CuI | 0.66 | 13.0 | High transparency and wide band gap (3.1 eV) | Insufficient stability | [12] |
| 03 | $NiO_x$ | 0.68 | 14.76 | large band gap, high optical transmittance and deep valence band well matched with perovskite layer | $NiO_x$ layers contain surface defects | [23] |

**Table 2-3** Summary of the synthesis sol-gel method of the NiOx based HTL PSCs device with different dopant

| S.NO | HTL | Synthesis Route | $V_{oc}$ | $J_{sc}$ | FF | PCE (%) | Ref |
|---|---|---|---|---|---|---|---|
| 01 | Cu-$NiO_x$ | Sol-gel method | 1.11 | 19.01 | 0.73 | 15.40 | [24] |
| 02 | Ag-$NiO_x$ | Sol-gel method | 1.08 | 19.70 | 0.80 | 16.86 | [25] |
| 03 | Zn-$NiO_x$ | Sol-gel method | 1.10 | 22.80 | 0.78 | 19.6 | [26] |
| 04 | Li-$NiO_x$ | Sol-gel method | 1.00 | 20.89 | 0.74 | 15.41 | [27] |
| 05 | Sr-$NiO_x$ | Sol-gel method | 1.11 | 22.73 | 0.79 | 20.05 | [28] |
| 06 | Cs-$NiO_x$ | Sol-gel method | 1.12 | 21.77 | 0.79 | 19.35 | [29] |
| 07 | Y-$NiO_x$ | Sol-gel method | 1.00 | 23.82 | 0.68 | 16.31 | [30] |
| 08 | La-$NiO_x$ | Sol-gel method | 1.01 | 21.02 | 0.73 | 15.46 | [31] |
| 09 | Li,Ag-$NiO_x$ | Sol-gel method | 1.13 | 21.29 | 0.80 | 19.24 | [32] |

### 2.4.3 Absorption layer

In PSCs, the perovskite absorption layer is a crucial part. The photoelectric properties of PSCs are dependent on perovskite's quality and morphology directly [33]. Perovskite material with the chemical formula $AMX_3$, such as $BaTiO_3$, $MAPbI_3$, $NaNbO_3$. Methylammonium ($CH_3NH_3PbI_3$) was used as light-harvesting material in perovskite solar cell by Kojima et al. in 2009. With reported high power conversion efficiency [8]. These efficiencies have been improving as much as 23% over the past few years. Unfortunately, organic-inorganic PSCs regardless of their high efficiencies and performances still suffer from certain degradations because of the weak level of the hydrogen bonding between monovalent organic cation and octahedral $PbI_2$ [34]. Such a PSC breaks down to $PbI_2$ under common external stresses, like electric charge, moisture, photo-oxidation, and UV irradiation.

Therefore, perovskite optimization is also a key to improving PCE. Based on previous work, the addition of additives, composition adjusting of precursors, modification on the surface, and deposition methods can affect the crystallization behavior of perovskite effectively [35].

## 2.5 Fabrication method of the perovskite thin-film layer

The chosen of a suitable fabrication procedure for the absorption layer of Perovskite solar cell is crucial because it impacts film morphology (surface coverage, shape, grain size, etc.), film thickness, crystallinity, and purity [36]. Serval method being used for fabrication of perovskite solar cell, but two main methods of fabrication are one-step solution processing by spin coating, two-step solution processing by spin coating, vapor assisted coating, vapor deposition, thermal vapor deposition method.

### 2.5.1 One step solution processing

In one-step solution processing method is the most popular technique for synthesis route of perovskite since the initial stage of perovskite research, in which pre-determined exact specific molar ratio of organic salt and lead halide are mixed in a solvent such as DMF/DMSO or a mixture of them. To make a single precursor solution and then afterward prepared solution spun on top of the glass substrate by using spin coater and the homogenous and uniform film is quickly annealed to transform the perovskite to solid-state and complete the perovskite formation. This technique is very simple and quick since it involves direct coating and conversion of the perovskite film by simply spinning on a spin-coater [37].

### 2.5.2 Two-step solution processing

Perovskite thin film layer can also be fabricated by a two-step solution processing method. Two-step coating for the synthesis of perovskite includes two distinct precursors solutions which are deposited on the substrate in a predetermined order. Usually, isopropanol IPA and DMF are used to dissolve the lead halide precursor and methylammonium iodide salt respectively. Initially, one precursor is spun on top of the substrate and then second deposited one of a few methods like dip coating, spin coating, vapor evaporation, and vacuum coating. This technique has been most preferred over the one-step solution

processing because of the better surface morphology of the perovskite layer which has allowed for higher efficiency to be obtained [38].

### 2.5.3 Vapor Assisted Solution Process

Synthesis of perovskite layer under Vapor Assisted Solution Process has first reported yang et al. it is novel low temperature and low-cost technique for the synthesis of a better quality of perovskite layer. The lead halide solution is deposited on to a glass substrate using a solution processing technique. The organic salt is vaporized at temperatures of 120-165 °C in an inert environment and the perovskite film grows on the substrate in a few hours [39] [40].

### 2.5.4 Thermal Vapor deposition

Vacuum deposition is another technique that can used be to deposit the light-harvesting layer and it is performed under vacuum, was first reported by Salau and then by Mitzi. The lead halides and organic salts are either deposited alternately or simultaneously on the substrate. The technique utilizes thermal evaporation with dual sources to form a perovskite layer High temperatures and suitable atmospheric conditions are required for this process [41, 42].

## Summary

In the last decade hybrid organic and inorganic PSC have acquired a lot of consideration due to efficient photovoltaic properties, high solar to PCE, and low processing cost, which make them a feasible candidate for PSCs. PSC possesses many attractive properties such as wide bandgap (3.5eV to 4.5eV), longer charge diffusion length, and higher optical absorbance excellent charge transport material. At the start of this chapter brief general introduction of perovskite material and the chemical formula was discussed and the structure of PSCs was explained in detail. After that briefly explained the device configuration regular (n-i-p) and inverted (p-i-n) and followed by the device working principle of PSCs. the preparation of PSC and its major three-layer HTL, light-harvesting (Absorber) layer, and ETL are briefly discussed with characteristics and properties. HTL materials were classified under the groups of organic and inorganic material doped with different metal oxides. The deposition route of the light-absorbing layer with different fabricating processes discusses briefly.

## References


1. Cheng, Z. and J. Lin, Layered organic–inorganic hybrid perovskites: structure, optical properties, film preparation, patterning and templating engineering. CrystEngComm, 2010. **12**(10): p. 2646-2662.
2. Watthage, S.C., et al., Chapter 3 - Evolution of Perovskite Solar Cells, in Perovskite Photovoltaics, S. Thomas and A. Thankappan, Editors. 2018, Academic Press. p. 43-88.
3. Sani, F., et al., Advancement on Lead-Free Organic-Inorganic Halide Perovskite Solar Cells: A Review. Materials, 2018. **11**(6).
4. Green, M.A., A. Ho-Baillie, and H.J. Snaith, The emergence of perovskite solar cells. Nature Photonics, 2014. **8**(7): p. 506-514.
5. Adjogri, S.J. and E.L. Meyer, A Review on Lead-Free Hybrid Halide Perovskites as Light Absorbers for Photovoltaic Applications Based on Their Structural, Optical, and Morphological Properties. 2020. **25**(21): p. 5039.
6. Yin, W.-J., et al., Halide perovskite materials for solar cells: a theoretical review. Journal of Materials Chemistry A, 2015. **3**(17): p. 8926-8942.
7. Mitzi, D.B., Templating and structural engineering in organic–inorganic perovskites. Journal of the Chemical Society, Dalton Transactions, 2001(1): p. 1-12.
8. Kojima, A., et al., Organometal Halide Perovskites as Visible-Light Sensitizers for Photovoltaic Cells. Journal of the American Chemical Society, 2009. **131**(17): p. 6050-6051.
9. Lee, M.M., et al., Efficient hybrid solar cells based on meso-superstructured organometal halide perovskites. Science, 2012. **338**(6107): p. 643-7.
10. Hussain, I., et al., Functional materials, device architecture, and flexibility of perovskite solar cell. Emergent Materials, 2018. **1**(3): p. 133-154.
11. Peumans, P., A. Yakimov, and S. Forrest, Small molecular weight organic thin-film photodetectors and solar cells. Journal of Applied Physics, 2003. **93**: p. 3693-3723.

12. Wang, H., et al., Efficient and Stable Inverted Planar Perovskite Solar Cells Employing CuI as Hole-Transporting Layer Prepared by Solid–Gas Transformation. Energy Technology, 2017. **5**(10): p. 1836-1843.
13. Chatterjee, S. and A.J. Pal, Introducing Cu2O Thin Films as a Hole-Transport Layer in Efficient Planar Perovskite Solar Cell Structures. The Journal of Physical Chemistry C, 2016. **120**(3): p. 1428-1437.
14. Jung, J.W., C.-C. Chueh, and A.K.Y. Jen, High-Performance Semitransparent Perovskite Solar Cells with 10% Power Conversion Efficiency and 25% Average Visible Transmittance Based on Transparent CuSCN as the Hole-Transporting Material. Advanced Energy Materials, 2015. **5**(17): p. 1500486.
15. Zhao, X., et al., Room-temperature-processed fullerene single-crystalline nanoparticles for high-performance flexible perovskite photovoltaics. Journal of Materials Chemistry A, 2019. **7**(4): p. 1509-1518.
16. Ge, J., C.R. Grice, and Y. Yan, Cu-based quaternary chalcogenide Cu2BaSnS4 thin films acting as hole transport layers in inverted perovskite CH3NH3PbI3 solar cells. Journal of Materials Chemistry A, 2017. **5**(6): p. 2920-2928.
17. Hu, Z., et al., Sol-gel-processed yttrium-doped NiO as hole transport layer in inverted perovskite solar cells for enhanced performance. Applied Surface Science, 2018. **441**: p. 258-264.
18. Xu, L., et al., Inverted perovskite solar cells employing doped NiO hole transport layers: A review. Nano Energy, 2019. **63**: p. 103860.
19. Zhao, Z., et al., Improving the Conductivity of PEDOT:PSS Hole Transport Layer in Polymer Solar Cells via Copper(II) Bromide Salt Doping. ACS Applied Materials & Interfaces, 2015. **7**(3): p. 1439-1448.
20. Burschka, J., et al., Sequential deposition as a route to high-performance perovskite-sensitized solar cells. Nature, 2013. **499**(7458): p. 316-319.
21. Jeon, N.J., et al., Solvent engineering for high-performance inorganic-organic hybrid perovskite solar cells. Nat Mater, 2014. **13**(9): p. 897-903.
22. Xu, L., et al., Improving the efficiency and stability of inverted perovskite solar cells by CuSCN-doped PEDOT:PSS. Solar Energy Materials and Solar Cells, 2020. **206**: p. 110316.

23. Islam, M.B., et al., NiOx Hole Transport Layer for Perovskite Solar Cells with Improved Stability and Reproducibility. ACS Omega, 2017. **2**(5): p. 2291-2299.
24. Kim, J.H., et al., High-performance and environmentally stable planar heterojunction perovskite solar cells based on a solution-processed copper-doped nickel oxide hole-transporting layer. Adv Mater, 2015. **27**(4): p. 695-701.
25. Jagadamma, L., et al., Efficient indoor p-i-n hybrid perovskite solar cells using low temperature solution processed NiO as hole extraction layers. 2019.
26. Zhu, W., et al., Aged Precursor Solution toward Low-Temperature Fabrication of Efficient Carbon-Based All-Inorganic Planar CsPbIBr2 Perovskite Solar Cells. ACS Applied Energy Materials, 2018. **1**(9): p. 4991-4997.
27. Park, M.A., et al., Enhanced electrical properties of Li-doped NiOx hole extraction layer in p-i-n type perovskite solar cells. Current Applied Physics, 2018. **18**: p. S55-S59.
28. Zhang, J.K., et al., Solution-processed Sr-doped NiOx as hole transport layer for efficient and stable perovskite solar cells. Solar Energy, 2018. **174**: p. 1133-1141.
29. Chen, W., et al., Cesium Doped NiOx as an Efficient Hole Extraction Layer for Inverted Planar Perovskite Solar Cells. Advanced Energy Materials, 2017. **7**(19): p. 1700722.
30. Hu, Z., et al., Sol-gel-processed yttrium-doped NiO as hole transport layer in inverted perovskite solar cells for enhanced performance. 2018. **441**: p. 258-264.
31. Teo, S., et al., The Role of Lanthanum in a Nickel Oxide-Based Inverted Perovskite Solar Cell for Efficiency and Stability Improvement. ChemSusChem, 2019. **12**(2): p. 518-526.
32. Xia, X., et al., Lithium and Silver Co-Doped Nickel Oxide Hole-Transporting Layer Boosting the Efficiency and Stability of Inverted Planar Perovskite Solar Cells. ACS Appl Mater Interfaces, 2018. **10**(51): p. 44501-44510.
33. Dunlap-Shohl, W.A., et al., Synthetic Approaches for Halide Perovskite Thin Films. Chemical Reviews, 2019. **119**(5): p. 3193-3295.
34. Ma, C. and N.-G. Park, A Realistic Methodology for 30% Efficient Perovskite Solar Cells. Chem, 2020. **6**(6): p. 1254-1264.

35. Milić, J.V., et al., Multifunctional molecular modulation for efficient and stable hybrid perovskite solar cells. 2019. **73**(4): p. 317-323.
36. Elseman, A., Organometal Halide Perovskites Thin Film and Their Impact on the Efficiency of Perovskite Solar Cells. 2018. p. 1-18.
37. Lv, M., et al., A promising alternative solvent of perovskite to induce rapid crystallization for high-efficiency photovoltaic devices. RSC Advances, 2015. **5**(26): p. 20521-20529.
38. Liang, K., D.B. Mitzi, and M.T. Prikas, Synthesis and Characterization of Organic−Inorganic Perovskite Thin Films Prepared Using a Versatile Two-Step Dipping Technique. Chemistry of Materials, 1998. **10**(1): p. 403-411.
39. Xiao, Z., et al., Efficient, high yield perovskite photovoltaic devices grown by interdiffusion of solution-processed precursor stacking layers. Energy & Environmental Science, 2014. **7**(8): p. 2619-2623.
40. Du, T., et al., Comparative Study of Vapor- and Solution-Crystallized Perovskite for Planar Heterojunction Solar Cells. ACS Applied Materials & Interfaces, 2015. **7**(5): p. 3382-3388.
41. Gao, P., M. Grätzel, and M.K. Nazeeruddin, Organohalide lead perovskites for photovoltaic applications. Energy & Environmental Science, 2014. **7**(8): p. 2448-2463.
42. Kim, B.-S., et al., Fully vacuum–processed perovskite solar cells with high open circuit voltage using MoO3/NPB as hole extraction layers. Organic Electronics, 2015. **17**: p. 102-106.

# Chapter 3: Materials and Methodology

## 3.1 Experimental Procedure

The experimental section of the study focuses on the synthesis of nanomaterials and their coating onto substrates to investigate their properties. The synthesis technique was chosen based on the requirements cost-efficient, ease of making, and availability. hence, the easy option for achieving our requirements was the sol-gel technique. With the help of the obtained results, some of the experimental conditions for the synthesized materials were continuously improved to achieve the optimum conditions and outcomes.

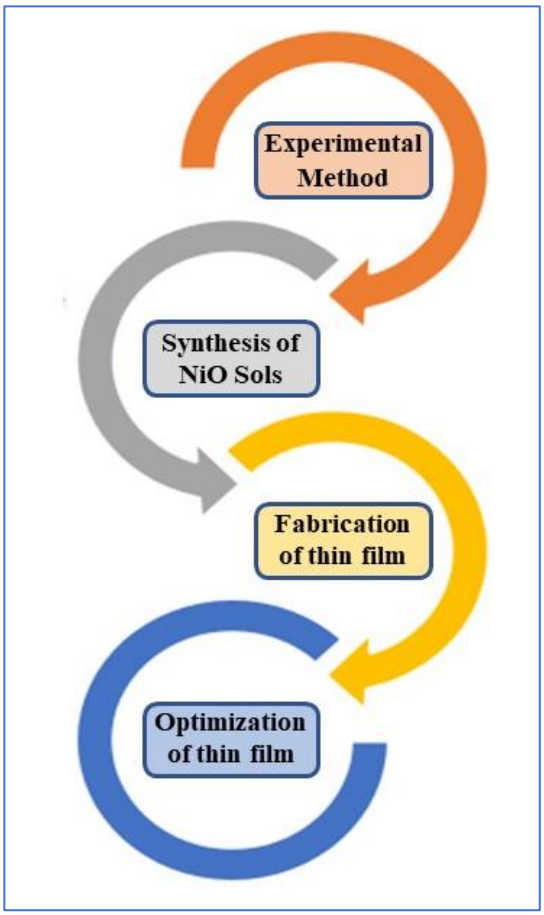


Figure 3-1 An overview of various steps of Experimental Methodology

## 3.2 Materials

Nickel acetate tetrahydrate (CAS No: 6018-89-9) Ethanolamine (CAS No: 141-43-5) 2-Methoxyethanol (CAS No: 109-86-4) and FTO conductive glass were purchased from Sigma Aldrich. Moreover, the Praseodymium (iii) nitrate salt was purchased from Alfa Aesar.

## 3.3 Deposition Technique of $NiO_x$ thin film

### 3.3.1 Pulsed laser deposition (PLD) Method

PLD is an immensely versatile method that's belonging to the physical vapor deposition category, which is used for depositing an epitaxial thin film of a wide category of material including polymers, semiconductors, metal, insulator, biological material, and high tech superconductor to acquire better quality thin films pulsed laser deposition technique categorized into three main steps 1) ablation of target material 2) creation and transport ablated plume and 3) condensation and film growth on the substrate [1]. A laser ablation technique is used in this procedure, which employs a very powerful density laser-focused by lenses to melt ionize and evaporate the coating material from target surface Coating.

In the initial phase, high-energy laser beams are focused on the surface of the target material inside a vacuum chamber, then the surface is heated up. Vapor is formed in front of the target material. The vaporization of the target surface region, which causes the removal of atoms from the target material, is a nonequilibrium process and is caused by the Coulomb explosion.

During the second phase, a bright plasma plume consists ideally of atoms, ions, electrons, and other small molecules, and particulates that quickly expand away from the surface of a target are created by the ablation process. In addition, the background pressure inside the chamber will have an effect on the spatial distribution of the plume. At the final phase, plume components impart the material flux, and it recondenses onto the substrate to form thin films [2].

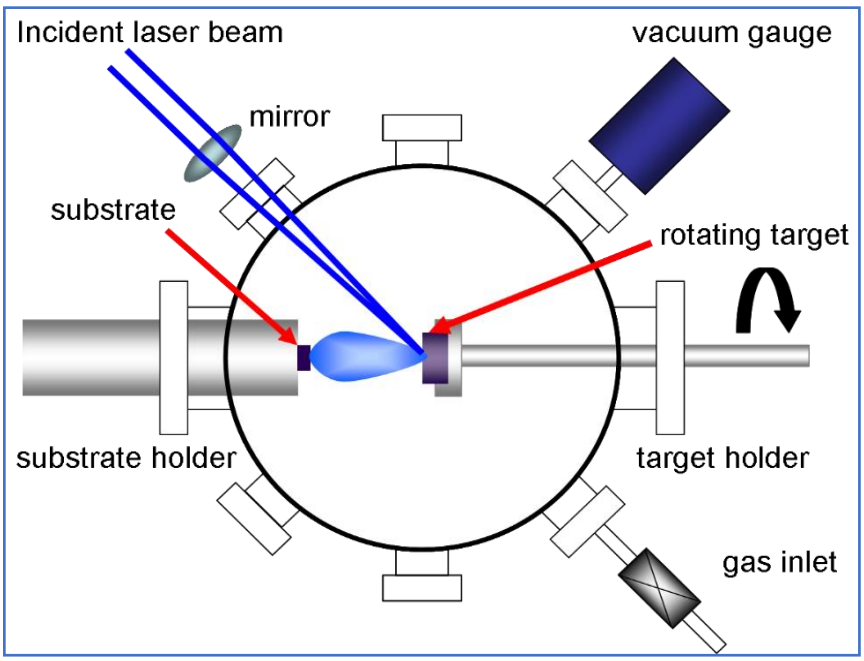


Figure 3-2 Schematic diagram of PLD system setup [3].

### 3.3.2 Chemical Spray pyrolysis Method

Chemical spray pyrolysis is one solution-based technique in which compounds of the constituents of the thin film are prepared by dissolving the appropriate metal salts and /or organometallics into an aqueous solution and atomizing the solution onto a heated substrate. Aside from the numerous alternative thin-film production techniques, this method is very simple and relatively cost-efficient. This adaptable approach can be used to create dense, porous, or multi-layered films of any composition.

substrate heater, spray nozzle, gas regulator, liquid pump, power supply, a compressed air source air compressor, and thermocouple temperature controller unit Liquid and gas flow regulators are used to control the flow of precursor solution and air. Liquid and gas flow regulators are used to control the flow of precursor solution and air. The spray nozzle, heater, and substrate holder are enclosed in a chamber and the outlet is fitted with an exhaust fan is installed in the exit to remove gases created during the disintegration of the spray solution [4].

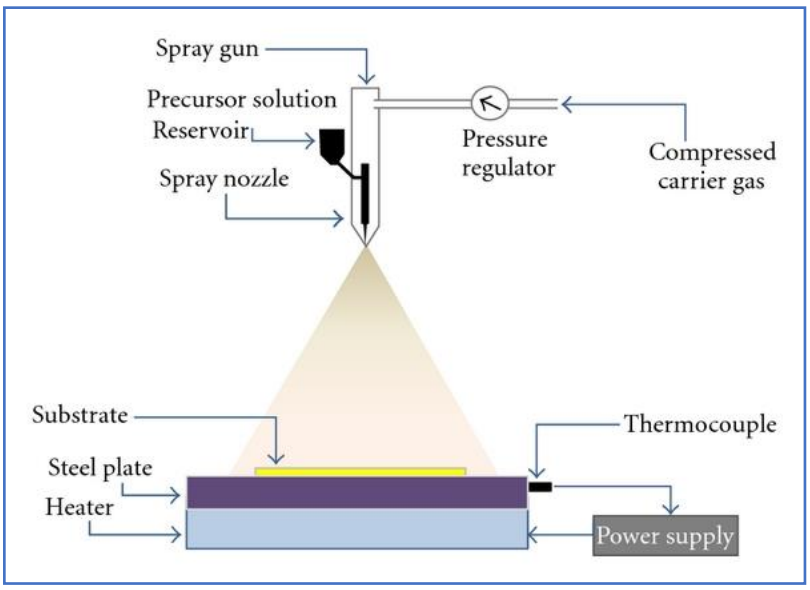


Figure 3-3 chemical spray pyrolysis setup [5].

### 3.3.3 Sputtering

Thin-film deposition techniques are categorized into chemical and physical methods. However, few techniques are based on glow discharges, and reactively sputtering is another kind of (PVD) physical vapor deposition method which involves the number of atoms ejected or sputtered off from the source or target material and deposition of these particles onto the substrate. The sputtering process is started when a substrate is placed in a vacuum chamber including an inert gas usually Argon and a negative charge is applied to a source that will be deposited onto the substrate, then the plasma glows.

Sputtering begins when a number of free-electron ejected from the cathode (negative charged) target surface or source in the environment of plasma striking with the outermost energy shell of argon gas and impelling these electrons off due to their same charge. Pressure is maintained inside the chamber for maximum collision between the electron and sputtering gas atom. With the increase in a collision, current increases which leads the plasma to become self-sustaining. To further maintain the plasma every electron has to maintain and produce sufficient secondary emission. In some cases, a collision can also result in glow discharge instead of ions production [6].

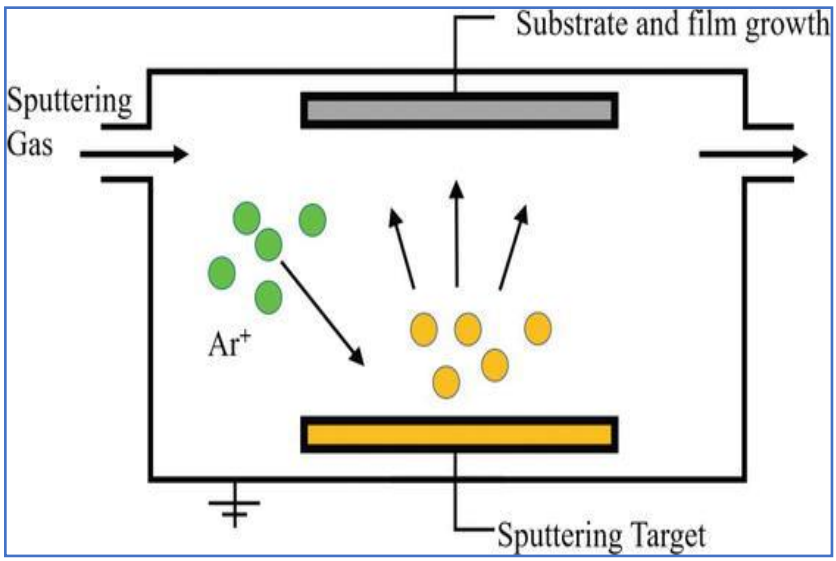


Figure 3-4 Working mechanism of the sputtering system [7].

Sputtering is classified into three types depending upon the power source as Radiofrequency (RF), High-power impulse magnetron sputtering (HIPIMS), and Direct current (DC). Sputtering is divided into different types such as magnetron sputtering DC or RF reactive, and ions assisted are mainly used for deposition of $NiO_x$ thin film [8].

### 3.3.4 Sol-gel method

Sol-gel processing is among the key deposition of the thin film technique in which Sol includes metal alkoxides as a precursor and their proper solvents. Furthermore, some useful additives, like stabilizers, may be included in sol. The sol is a system in which separate chemical species solvent and solute are metastable. If suspension conditions are changed slightly, destabilization can occur. The destabilization of sol can result in the precipitation of sols species as aggregated or unaggregated particles in the formation of a homogeneous gel. The liquid-filled solid network known as 'gel' is formed by joining colloidal particles in a three-dimensional structure. Changing the pH value of the sol with catalysts such as acids and bases is the most typical way to induce the transformation from sol to gel [9].

### 3.3.5 Sol-gel method-based Coating techniques

#### 3.3.5.1 Dip coating

Dip coating is a very easy and antiquated technique that can be used for immersion of a substrate into coating sol and later withdrawing of the substrate from sol from deposition of the thin film. The film thickness depends on the viscosity of the solution, surface tension, and gravity [10]. It also depends upon the immersion time of substrate into coating solution, the more rapid substrate withdrawal causes the thicker film This method allows both sides of the substrate to be coated at the same time, The deposition of sol onto curved or complex-shaped substrates is possible with large-scale thin-film fabrication.

Dip coating can be categorized into the following steps.

**Immersion:**

The first step of the process is immersed of the substrate into a solution of desirable coating material at constate speed

**Hold Time:**

The substrate should be dipped into the solution for a known time duration. Time duration of immersion of substrate affects the thickness and is then drawn up with constant speed.

**Deposition:**

When the substrate is drawn up thin layer deposits itself on the substrate. The withdrawal of substrates should be carried out at a constant speed for getting uniform films.

**Drainage:**

After pulling up the substrate the excess liquid will drain from the substrate surface.

**Evaporation:**

finally, the substrate is annealed at a suitable temperature for evaporating the solvents forming thin films.

#### 3.3.5.2 Spray coating

spray coating is a technique in which uses a spray of fine particles or droplets that deposits material onto the surface of the material. Deposition characteristics such as scanning speed and spray pressure can be controlled. Important deposition characteristics are the

sol's boiling temperature and the wetness of the substrate surface. It allows for deposition on complex surfaces. It is an effective and extensively used coating process in the industry [11].

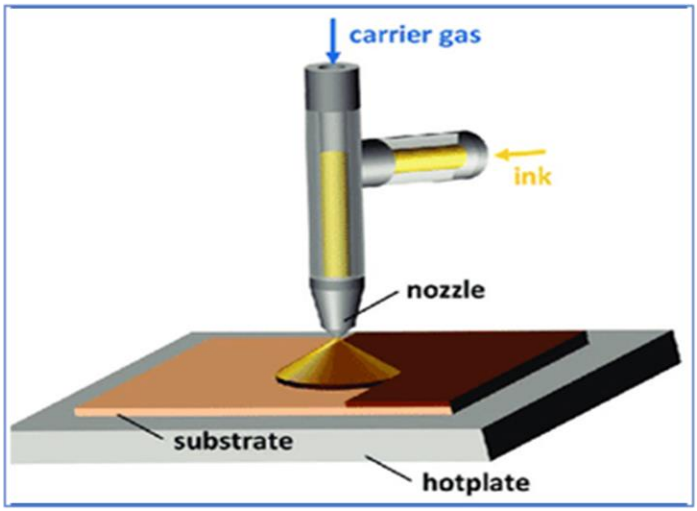


Figure 3-5 Schematic diagram of spray coating technique [12]

### 3.3.5.2 Spin coating

Spin coating is an extensive procedure that is employed to acquire quite dense, uniform, and high-quality thin films on the desired surface. The spin coating technique normally includes the application of thin-film thickness ranging from only a few micrometers (um) to nanometers (nm) on a flat, uniform substrate surface. The spin coating allows for the quick, easy, and repeatable fabrication of single/multi-layered thin films. It is mainly used in a plethora of technological applications and industries. The advantages of this technique are easy and quick, and the limitation of this technology is that it can only be used on flat surfaces. [13, 14].

The desirable thin film remains on a flat substrate after a few rotations. For the required film, the coating flow is dominated by centrifugal force, and Coriolis force and gravity are negligible. The centrifugal force spreads the solution into a thin layer, from which the solvent quickly evaporates, leaving a homogeneous solid coating on the substrate. The substrate radius is always greater than the required film thickness thus the lubrication approximation holds. Following are four steps which are comprised of spin coating technique such as deposition, spin-up, spin-off, and evaporation.

**Deposition:** Deposition step to obtain the excess amount of coating solution which entirely covers the flat substrate.

**Spin up:** Spin up a step, a certain spin speed will be applied to dispense the solvent gradually on the substrate surface. Typically, the spinning speed applied at this step is below 1000 rpm. This will create a fairly uniform thin layer of film on the substrate surface.

**Spin-off:** Spin-off step, substrate starts rotating at a constant speed, a higher spinning speed will be applied to accelerate the solvent to spread wider on the substrate surface.

**Evaporation step:** The evaporation step causes the thinning of the coating layer. Finally, substrate is annealed on the suitable temperature for evaporating the solvents forming thin films.

## 3.4 Preparation of $NiO_x$ Sols

Nickel acetate tetrahydrate $(NiCH_3OO)_2.4H_2O$ act as primary precursor salt for the synthesis of $NiO_x$ (sols), while 2-Methoxyethanol ($C_3H_8O_2$) used as a solvent and Monoethanolamine works as a stabilizing agent molar ration, were kept maintaining at 1:1:1 for Nickel acetate tetrahydrate salt, MEA and ME respectively. These chemicals were mixed in a sealed glass vial at the same time in ambient environmental conditions. The mixture in the glass vial was stirred at 135 °C temperature for 10 hours. Moreover, followed by a syringe filter with a pore size of 0.45μm.

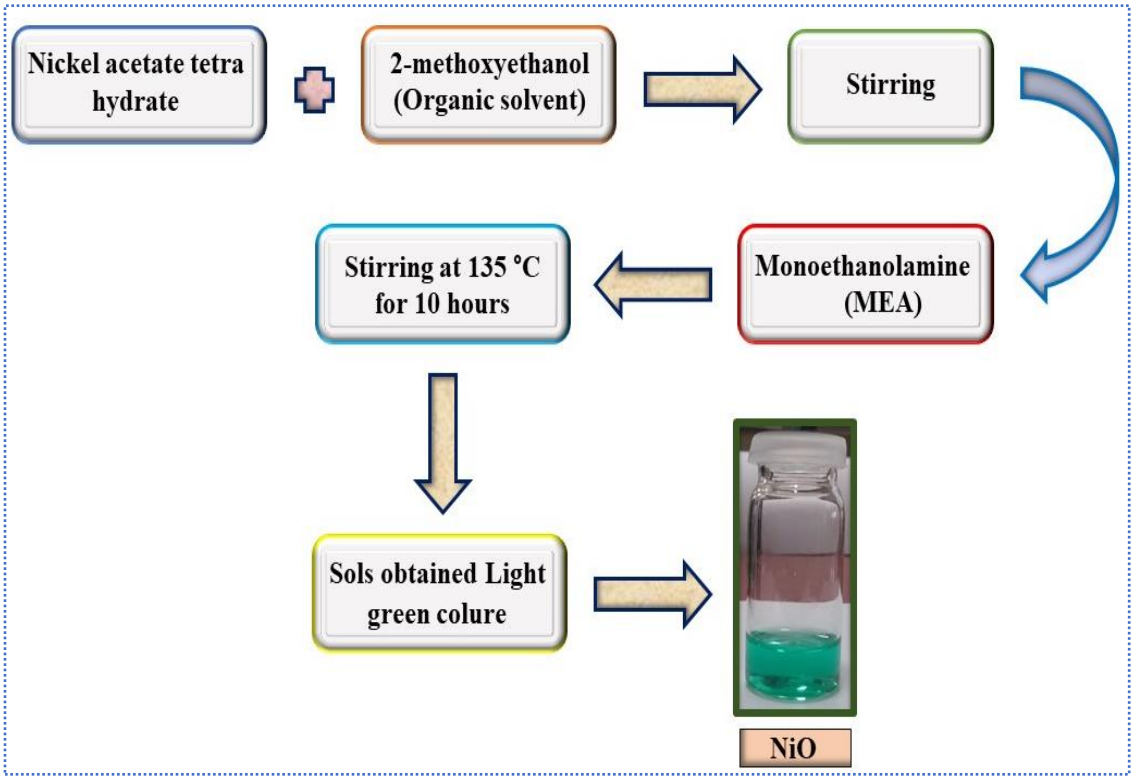


Figure 3-6 Process flow diagram of the synthesis of Nickel oxide (NiOx) sols

## 3.5 Synthesis of Pr doped $NiO_x$ Sols

For the synthesis of Pr doped $NiO_x$ sols, the utilized method was used remarkably much like the one used in the previous section. The prominent difference here to be considered is the use of Praseodymium as a precursor salt with different molar concentrations ( 0, 2, 4, and 6 mol% ) furthermore Nickel acetate tetrahydrate act as organic salt, 2-Methoxyethanol used as an organic solvent, and MEA act as a stabilizing agent. molar ratios were kept maintained the same. the remaining method was kept the same.

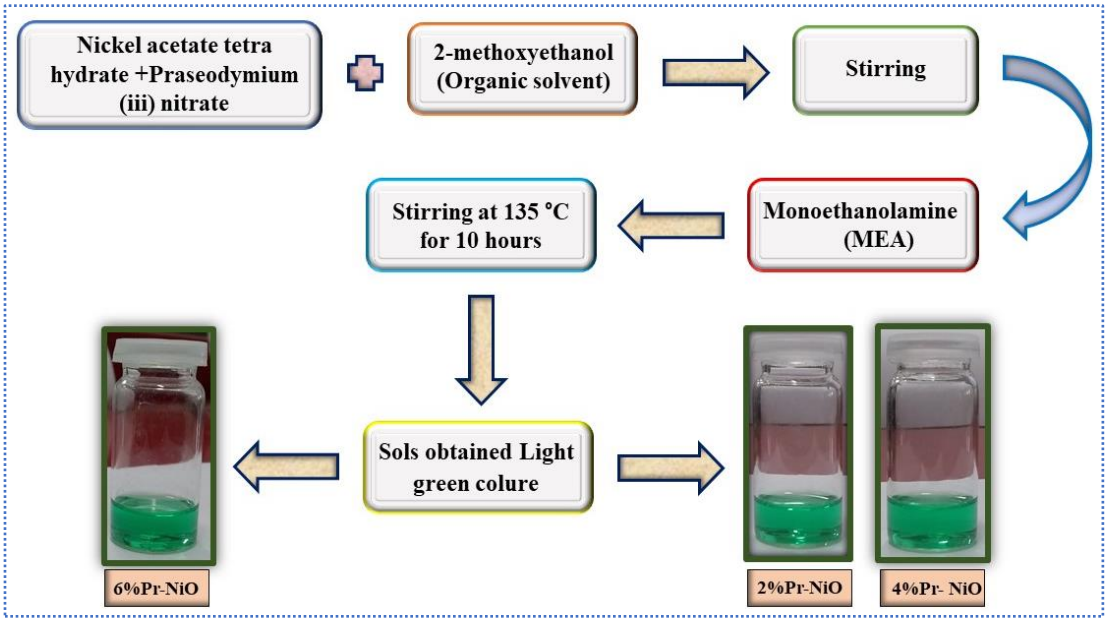


Figure 3-7 Process flow diagram of the synthesis of different concentrations of (2,4, and 6 mol%) Pr-doped NiOx sols

## 3.6 Deposition of thin film

To make $NiO_x$ and Pr-$NiO_x$ thin film from synthesized sols, the method of the spin coating was chosen. The selection of this procedure was based on the thickness requirements of thin films for the specified applications along with its simplicity and easy arability.

Deposition of undoped and Pr-doped $NiO_x$ thin films hole transport layer on patterned FTO glass substrates by the spin coating technique under ambient condition, before deposition FTO glass was washed stepwise by ultrasonication in DI-water, detergent, Isopropanol, Absolute Ethanol, and acetone for 15 minutes respectively, after being dried at 70 °C for 1 hr in drying oven, then the substrates were taken out of the beaker and then give Plasma cleaning treatment for 15 minutes. to remove organic materials. The $NiO_x$ and Pr-$NiO_x$ precursor solutions were then filtered through a syringe filter with pore size 0.45µm. The prepared precursor solution was deposited on the FTO glass substrate at 3000 rpm for 40 sec and after that preheated at 135 °C for 10 minutes on a hot plate after preheating to evaporate the solvent and any remaining organic compounds. The FTO conductive glass substrate was transferred into the furnace for annealing at 450 °C for 1

hr with the ramping rate of 1 °C $min^{-1}$ in ambient condition to get the required thin film of $NiO_x$ and Pr-doped $NiO_x$.

After FTO substrates were cooled down at ambient temperature then films were transferred into the glovebox ($O_2$ and $H_2O \leq 0.1$ ppm**)** the precursor solution was spin-casted onto the undoped and Pr-doped $NiO_x$ thin film layer via a consecutive two-step spin-coating procedure at 1000 rpm and 5000 rpm for 10 sec and 20 sec, accordingly. In the second step, 300 µL of ($C_6H_5Cl$) chlorobenzene as antisolvent drop-casting was rapidly dropped onto the middle of the spinning substrate at starting of program 10 sec. the prepared samples were dried on hot-plate 100 °C for 1 hour in a glove box filled with nitrogen to obtained required dark brown films. Afterward, already prepared perovskite thin film was individually spin-coated by electron transport material PCBM (20 mg m/l) possessing 2 weight percent of Tetrabutylammonium tetrafluoroborate (TBABF4) in anhydrous chlorobenzene via spin casting at 3000 rpm for 30 sec and dried at 100 °C for 10 min. afterward, the PCBM layer was spin-coated by 0.1 weight percent of TIPD in Isopropyl alcohol (IPA) at 5000 rpm for 30 sec, then vacuum dried. At last, Silver (Ag) electrodes with a thickness of 100 nm were deposited by thermal evaporation at 6 x $10^{-6}$ torr. Device active area is specified at approximately 1.2 $cm^2$ by the shadow mask.

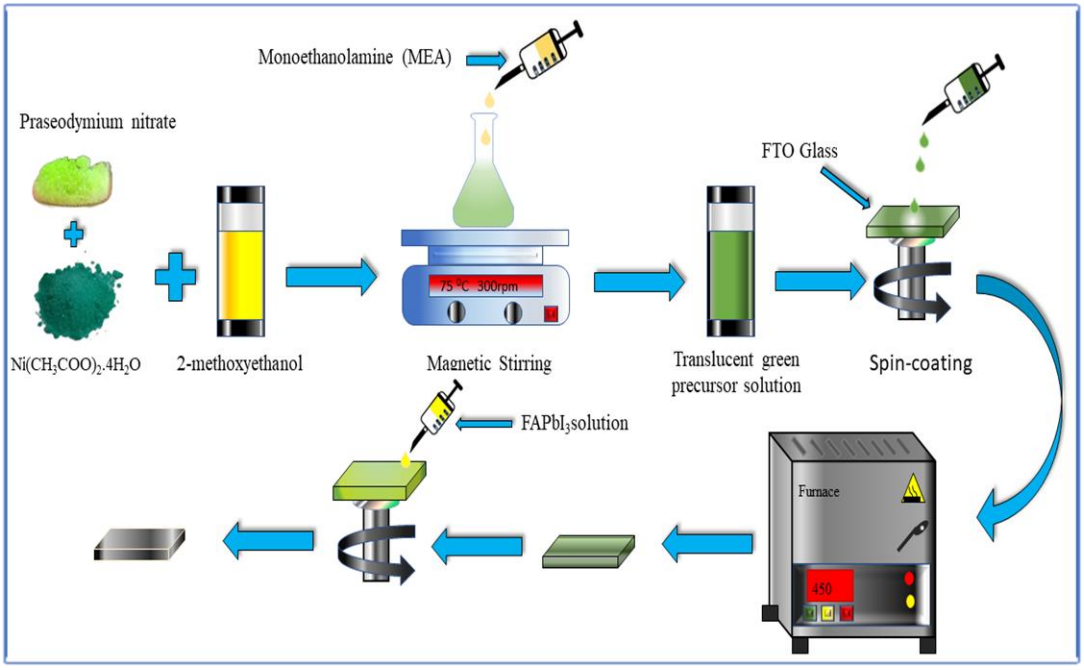


Figure 3-8 Schematic illustration of the sol-gel process and device fabrication.

## 3.7 Characterization and Techniques Overview

### 3.7.1 X-rays Diffraction

XRD is a systematic and non-destructive technique utilized for orientation and phase identification of crystalline materials and evaluating crystal structure, phase change, dimension of a unit cell, and lattice parameter of the desired sample. XRD is also used to determine structural properties such as crystal defect, grain size, microstrain, and epitaxy Constructive interference produces the diffraction peaks of X-ray beams coming from each lane of a crystal lattice in a sample at specific angles [15]. When crystalline materials are illuminated by a monochromatic x-ray beam, which interacts with the atoms of material and refracts x-rays characteristic energy. To reveal the XRD pattern, they are subjected to constructive interference The source of x-rays is the cathode tube which filters, directs, and concentrates the rays to the sample. The lattice spacing is then derived using Bragg's law

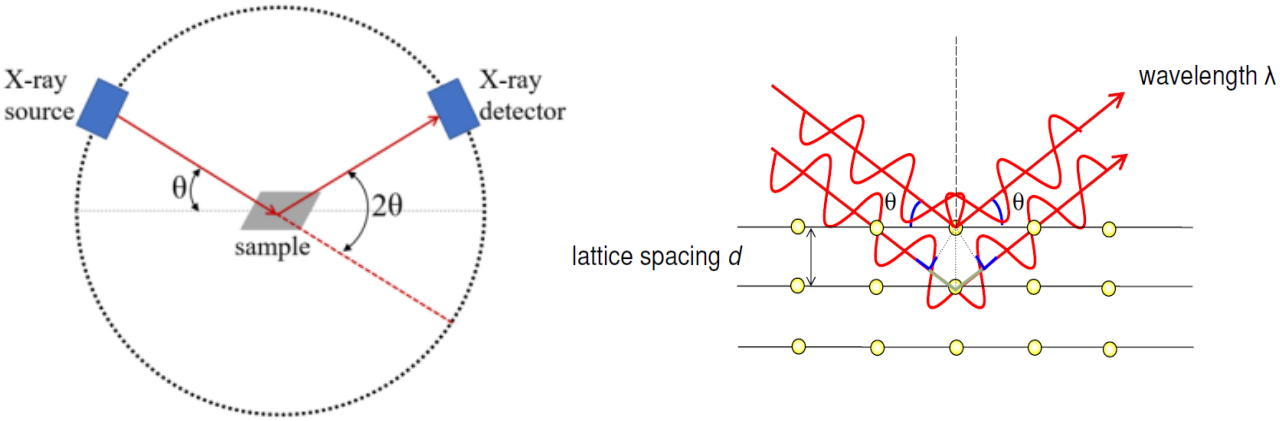


Figure 3-9 (a) shows (left image) Schematics of XRD measurements and (b) shows (Right image) Constructive interference on a crystal plane

$$n\lambda = 2d \sin\theta$$

$n$ is an integer value.

$\lambda$ is x-rays wavelength.

d is the interplanar distance between the atomic planes of material.

θ is the angle difference between the incident ray and the plane normal.

Also, the crystallite size was calculated using the Scherrer formula. 'D' is given by

$$d = \frac{k\lambda}{\beta \cos \theta}$$

Here "λ" is the wavelength in nm, "θ" is the diffraction angle, and "β" is the full width half maximum. k = a constant having the value of 0.94. Also, x-ray gives the aggregate data of crystallite sizes and in most cases, it does not follow standard patterns for a sizeable measure of powder.

### 3.7.2 Scanning Electron Microscope (SEM)

SEM is a technique to examine surface morphology of thin-film and the shape of particles and powders. A simple microscope magnifies any material surface using visible light with a high magnification capacity. Because an electron beam is utilized instead of visible light in SEM, it may achieve magnifications of up to 300,000X and a probing depth of 10 nm to 1 μm.

**Working Principle**

The electron beam is generated thermionically by using an electron gun fixed on a tungsten filament cathode. The tungsten metal has the highest melting point and lowest vapor pressure so it can be used for electron beam generation via heating thermionic electron guns. The electrons in the beam could interact with the atom inside the sample, producing a variety of signals which can be used for collecting information about the samples including the surface topography and composition. The secondary electrons are collected for the most common SEM mode for showing the morphology and topography of samples, at the same time the backscattered electrons are valuable for illustrating contrast in composition, and x-rays are commonly used for the elemental analysis [16].

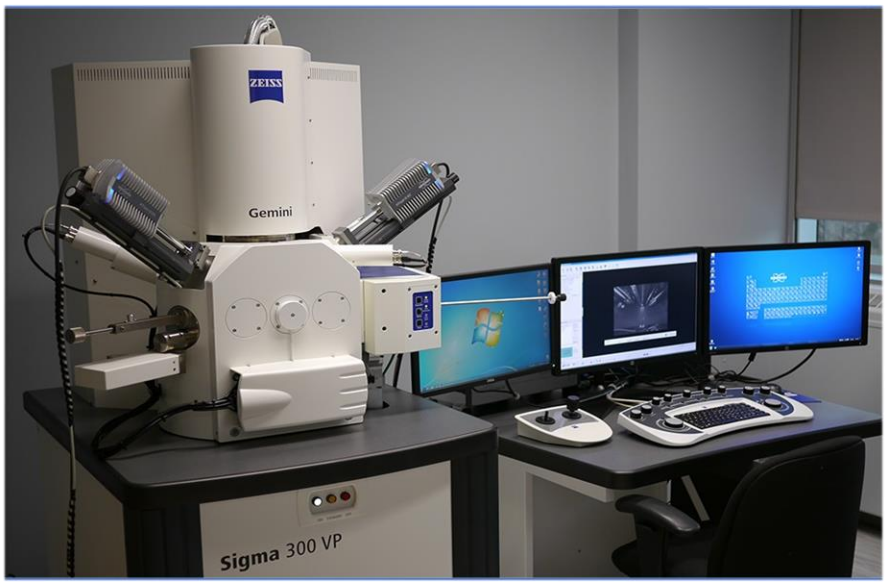


Figure 3-10 Scanning Electron Microscope

### 3.7.3 Energy Dispersive spectroscopy (EDS)

The analytical technique of EDS allows information on the Chemical and elemental composition of sample such as phase separation, distinguishing different composition layers. It interacts with the atoms of the sample using an electron beam similar to that used in SEM. However, the EDS spectra that it produces results from the x-rays emitted from sample. When sample is bombarded with a source of high-energy electrons or protons, the atoms on surface of sample eject electrons resulting in generation of vacancies in the structure. These vacancies are subsequently filled with electrons from higher energy states releasing x-ray. These x-rays are distinctive for each element. EDS/EDX is usually combined with the SEM unit. The detector in EDS records the abundance of x-rays emitted from sample versus their energy, thus, resulting in an EDS spectrum.

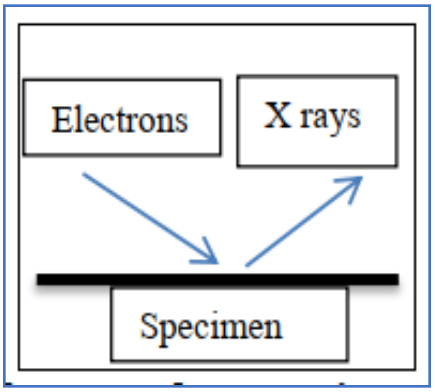


Figure 3-11 Probe beam and measuring particle in EDS

### 3.7.4 Atomic Force Microscopy (AFM)

AFM is a surface analysis technique which is useful for examining the coating at micro and nano range and measuring the height and thickness of nano-compound. The AFM can be used for high resolution imaging of many different surfaces to determine surface morphology, roughness and texture. The tip senses the chemical atoms by forming chemical bonds with them. The interactions alter the vibrational frequency, and these changes are mapped out by the program.

A typical AFM consists of a cantilever with a sharp small tip (acting as the probe) at free end, a laser, a 4-quadrant photodiode, and a scanner. When the tip of the cantilever, which is attached to free end, comes very close to the surface, attractive and repulsive forces owing to interactions between the tip and the sample surface cause the cantilever to bend negatively or positively. This bending can be detected with the help of a laser beam. The tip slides up and down as it goes across the sample, depending on the sample's surface properties(e.g., topography). The piezoelectric scanner is used to scan the sample surface. A feedback control mechanism keeps the distance between the tip and the surface of the sample constant. Optical lever monitors deflections from laser source on cantilever’s back which is read by a sensitive photodiode. Vertical resolution is up to sub-A° and lateral dimensions are up to 1 nm.

### 3.7.4.1 Modes of operation AFM

**Tapping mode:** In this tapping mode operation, the AFM tip is in intermittent contact with the sample surface by keeping the amplitude of oscillation of the tip constant through feedback. Topography (height), phase, and amplitude are the three channels through which data is collected (or error signal). This allows the mapping of high roughness surfaces without damaging AFM tip.

**Contact mode:** In this contact mode operation, the AFM tip is in constant contact and scanned across the sample surface. The feedback system aims to keep the AFM cantilever deflection is constant and subsequently constant interaction force. In this way, repulsive force is experienced by the AFM tip and sample surface. Soft AFM cantilevers of less than 1 N/M are commonly utilized to reduce AFM tip wear and surface damage while also increasing sensitivity.

**Non-contact mode:** In this mode of operation sample to tip, distance is maintained in the range of a few hundreds of Å. A larger distance develops weak attractive forces between the tip and sample surface rather than repulsive forces.

### 3.7.5 Ultraviolet-Visible (UV-VIS) Spectroscopy

UV-vis spectroscopy performs optical spectroscopy to investigate how light interacts with matter in the ultraviolet (190 nm - 400 nm) and the visible (400 nm - 700nm) range of light, which is related to the electronic transitions from the ground state to the excited state of atoms or molecules and which assist to identify the existence of heteroatoms, impurities, saturation or unsaturation in material [17].

### The Principle of operation

When a sample is placed under the UV-Vis spectrum the electrons get excited to higher antibonding orbitals. Lesser the energy gap between HOMO and LUMO of a material, easier is the excitation of electrons by longer wavelength radiations with a wavelength corresponding to that energy, the electron is jumped from HOMO to LUMO. This is referred to as electronic transition to anti-bonding and is denoted by $\sigma - \sigma^*$. The graph between absorption or transmittance of light on the X-axis and different wavelengths on the Y-axis is obtained and analyzed [18].

### 3.7.6 Hall Effect measurement

The electrical properties of semiconductor thin films, such as charge carrier type and density, mobility, conductivity, resistivity, and sheet resistance, are determined using a Hall Effect measurement system. Edwin H. Hall, an American physicist, discovered this effect in 1879. Hall Effect measurement system work on the principle of Lorentz force. The direction of the magnetic force is determined by the right-hand rule, i.e., in the opposite direction in which the thumb is pointed. In this case, the Lorentz force is the combination of both electric and magnetic force and is calculated as, **- q(E + v x B)** where E is electric field and B is magnetic field  When a potential difference is applied across a conductor, current starts to flow which is a combination of electrons, holes, or ions. When a perpendicular magnetic field is applied, these charge carriers experience a force, called Lorentz Force, which makes these charges bend from their path making equal and opposite charges on contrasting faces. This parting of charges creates an electric field which hinders the movement of more charges, so a stable electric potential is built till the charges are flowing.

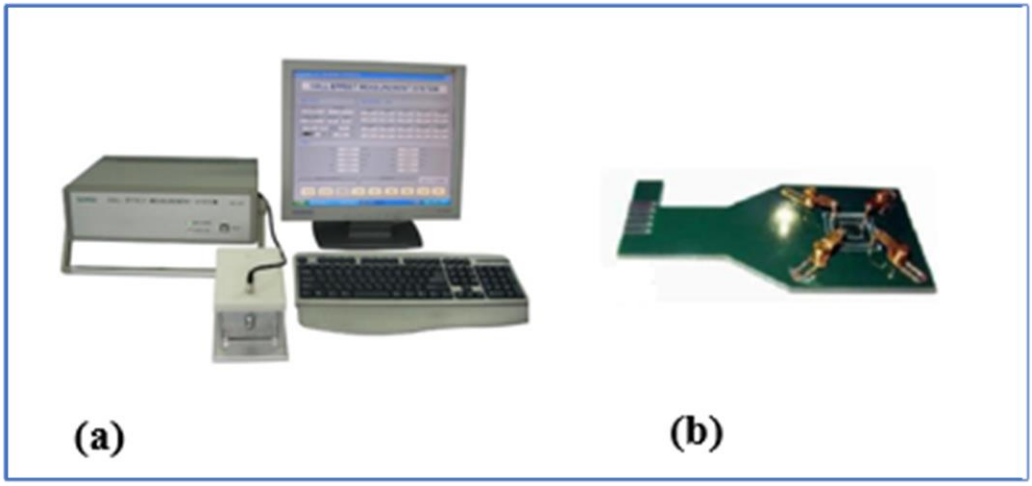


Figure 3-12 (a) Hall effect measurement System (b) Sample holder

### 3.7.7 Non-contact Profilometer

The film thickness was measured by using an optical profilometer. It was based on a non-contact mode instrument employing 2D Nonovea software and the average height of film

thickness was measured using a scanning length of 12 mm. The analysis is used to determine the surface roughness and fractality

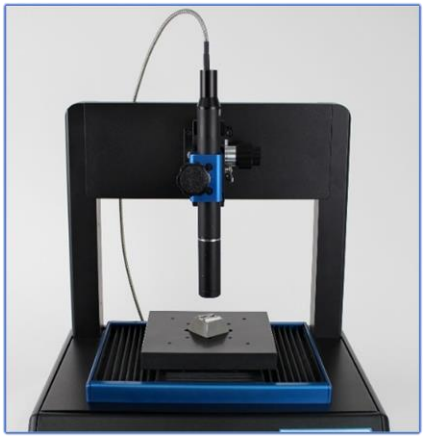

Figure 3-13 A non-contact profilometer

### 3.7.8 Hydrophobicity measurement

Thomas Young was initially calculated the contact angle of water droplets, who depicted a droplet's static contact angle on a plane surface, super-hydrophilic or super-wetting surface has contact angle less than 30°. A 5 µm water droplet was poured onto the surface of fabricated layers to calculate the droplet's contact angle with the surface. In general, the surfaces generating an angle of more than 90° are referred to as hydrophobic but with keeping view the viscosity of water, any angle closer to 90° is highly hydrophobic.

Figure 3-14 Schematic illustrations of Contact angle measurement

### 3.7.9 Measurement of photovoltaic properties

To evaluate the fabricated solar cells' electrical performance as well as their current density, efficiency, open current-voltage (Voc), and fill factor (FF) is measured by JV curve system as shown in the diagram.

## Summary

This chapter explained the facile and effective method of material synthesis of Pr-doped $NiO_x$, and fabrication of PSC device. Different thin film deposition coating techniques are briefly explained such as PLD, CSD, sputtering, and sol-gel solution-based technique such as dip coating, spray coating, and spin coating. In which PLD, CSD, and sputtering techniques are comparatively expensive vacuum-based techniques. They required to require high and ultra-high vacuum for deposition technique. Whereas solution-based (Sol-gel) wet chemistry routes are cheap and clean can be done with simple apparatus and no high vacuum is required and can be done in low or no vacuum. This spin coating is quick, easy, and reproducible because it is a low-cost solution-based technique therefore, it is mainly employed in different industries and photovoltaic technologies applications. The spin coater was used to spin the prepared sols on top of the FTO glass substrate to acquire the thin film deposition. It rotates at high speed to allow the solution to fly off and spread evenly on the glass slide. The thickness of films is dependent on the rotational speed of the spin coater. In this chapter a review on the detail of the working of different characterization and testing techniques utilized such as XRD, SEM/EDS, AFM, UV-Vis spectrometry, Hall effect measurement system, optical profilometry, Hydrophobicity measurement, and J-V curve measurement.

## References


1. Pilban-Jahromi, S., et al., Facile Synthesis of Porous-Structured Nickel OxideThin Film by Pulsed Laser Deposition. Journal of Nanomaterials, 2012. **2012**.
2. Wang, K.J.A.i.G.S., Laser based fabrication of graphene. 2013: p. 77-95.
3. " laser based fabrication of graphene" " [Online]. Available from: https://www.intechopen.com/chapters/45025 / [Accessed: 12-Nov-2019].
4. Patil, G., et al., Spray Pyrolysis Deposition of Nanostructured Tin Oxide Thin Films. ISRN Nanotechnology, 2012. **2012**.
5. Patil, G.E., et al., Spray Pyrolysis Deposition of Nanostructured Tin Oxide Thin Films. 2012. **2012**: p. 1-5.
6. Depla, D., S. Mahieu, and J.E. Greene, Chapter 5 - Sputter Deposition Processes, in Handbook of Deposition Technologies for Films and Coatings (Third Edition), P.M. Martin, Editor. 2010, William Andrew Publishing: Boston. p. 253-296.
7. "Ampersand tutorial" [Online]. Available from: https://ampersandtutorials.com/nano-technology/thin-film-deposition/ [Accessed: 12-Nov-2019].
8. Shi, F., Introductory Chapter: Basic Theory of Magnetron Sputtering, in Magnetron Sputtering. 2018.
9. Danks, A.E., S.R. Hall, and Z. Schnepp, The evolution of 'sol–gel' chemistry as a technique for materials synthesis. Materials Horizons, 2016. **3**(2): p. 91-112.
10. Lee, J.W., S.I. Na, and S.S. Kim, Efficient spin-coating-free planar heterojunction perovskite solar cells fabricated with successive brush-painting. Journal of Power Sources, 2017. **339**: p. 33-40.
11. "Nadetech Innovations." [Online]. . Available from: https://nadetech.com/products/dip-coating [Accessed: 21-Dec-2016]
12. Zafar, M.J., D. Zhu, and Z. Zhang, 3D Printing of Bioceramics for Bone Tissue Engineering. Materials, 2019. **12**(20).
13. "Spin Coating: Complete Guide to Theory and Techniques." | Ossila. [Online]. Available from: https://www.ossila.com/pages/spin-coating#introduction-to-spin-coating. [Accessed: 02-Nov-2021].

14. Howard, I.A., et al., Coated and Printed Perovskites for Photovoltaic Applications. Advanced Materials, 2019. **31**(26): p. 1806702.
15. “X-Ray Diffraction - an overview | ScienceDirect Topics.” [Online]. Available from: https://www.sciencedirect.com/topics/materials-science/x-ray-diffraction. [Accessed:04-Nov-2021].
16. J. I. Goldstein, D.E.N., J. R. Michael, N. W. M. Ritchie, J. H. J. Scott, and D. C. Joy,, Scanning electron microscopy and X-ray microanalysis. Springer, 2018.
17. D. A. Skoog, F.J.H., and S. R. Crouch,, Principles of instrumental analysis, 6th ed.Belmont, CA: Thomson Brooks/Cole, 2007.
18. H.-H. Perkampus,UV-VIS Spectroscopy and its Applications. Springer Science & Business Media, 2013.

# Chapter 4: Results and Discussion

The effect of doping of Praseodymium on the structural, morphological, electrical, electronic, and optoelectronic properties of HTL in inverted structure of PSC is examined in this result and discussion chapter. Undoped and Pr-doped $NiO_x$ thin film was deposited on FTO conductive glass substrate and characterized by XRD, SEM, EDS, AFM, UV-VIS, Hall effect, Contact angle, and current-density voltage (J-V) curve.

## 4.1 Structural Analysis

To investigate the structure of the Thin-Films, XRD studies were carried out where the important parameters of the $NiO_x$ and Pr-doped $NiO_x$ samples were analyzed in depth. This technique is significant due to the results XRD produces, which facilitates a better understanding of the crystal structure and how the doped atom in the host lattice affects the lattice parameters of the host material.

### 4.1.1 X-ray diffraction (XRD)

XRD results are shown in Fig 4.1 for undoped $NiO_x$ and different doping concentrations 2, 4, and 6 mol% Pr-doped $NiO_x$ along with three prominent diffraction peaks at **37.4°, 43.4°, 63.0°** correspond to (**1 1 1**), (**2 0 0**), and (**2 2 0**) diffraction planes, respectively with the space group of Fm3m and space group number 225. the pattern of XRD peaks in accordance with (JCPDS No.47-1049). The measuring mode was 'θ-2θ' which scanned the range 20°-75° using the Cu kα source of λ = 0.154nm. the scan step was set at 0.04° and the source (40 kV and 40 mA), respectively. From the peak matching and peak sharpness, the highly crystalline nature of the material is evident. No impurity peaks were detected within the detection limit of XRD such as $Pr_2O_3$ and $PrNiO_3$. This confirms that the $NiO_x$ structure was not disturbed, and Pr was incorporated into the $NiO_x$ latticed structure. Here, it can be noted that XRD peaks are widened denoting the reduced size of the crystal as enhancing the concentration of Pr-ions.

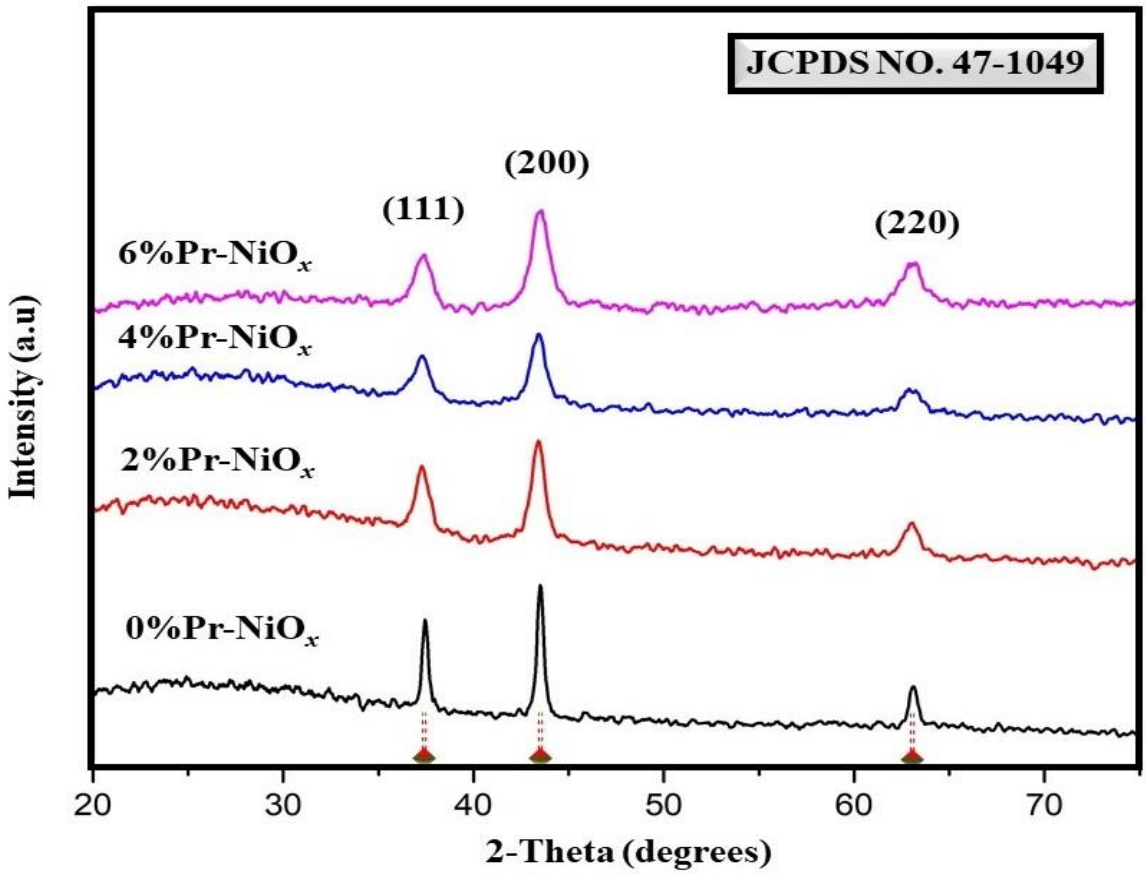


Figure 4-1 XRD pattern of 0%Pr-doped, NiOx, 2%Pr-doped NiOx, 4%Pr-doped NiOx, and 6%Pr-doped NiOx

The average crystallite size of undoped $NiO_x$ and Pr-doped $NiO_x$ was calculated by using the renowned Scherrer equation as shown in Table 4.1 and crystallite size summarized in Fig 4.2 it has been found in between the range of 28 nm to 12 nm after incorporating Pr-ions. Furthermore, lattice parameter value rises markedly from 4.1622 Å for undoped $NiO_x$ to 4.1696 Å for 6% Pr doped $NiO_x$ denoting lattice expansion which successfully confirms incorporation of Pr-ions. as $Pr^{3+}$ (from precursor) possesses a higher ionic radius of [0.113 nm] compared to that of $Ni^{2+}$ of [0.069 nm] and the position of (200) peak shifted toward the diffraction angles with increasing doping concentration [1, 2].

Table 4-1 XRD table showing the diffraction data of at 200 peaks, using the Debye-Sherrer formula to calculate the average crystallite size of undoped NiOx and Pr-doped NiOx thin films.

| Sample | 2-theta | FWHM | D(nm) | Lattice Parameter |
|---|---|---|---|---|
| 0%Pr-$NiO_x$ | 43.483 | 0.295 | 28.69199 | 4.162252284 |
| 2%Pr-$NiO_x$ | 43.435 | 0.394 | 21.47899 | 4.166629199 |
| 4%Pr-$NiO_x$ | 43.424 | 0.689 | 12.28215 | 4.167633642 |
| 6%Pr-$NiO_x$ | 43.402 | 0.695 | 12.17519 | 4.169644096 |

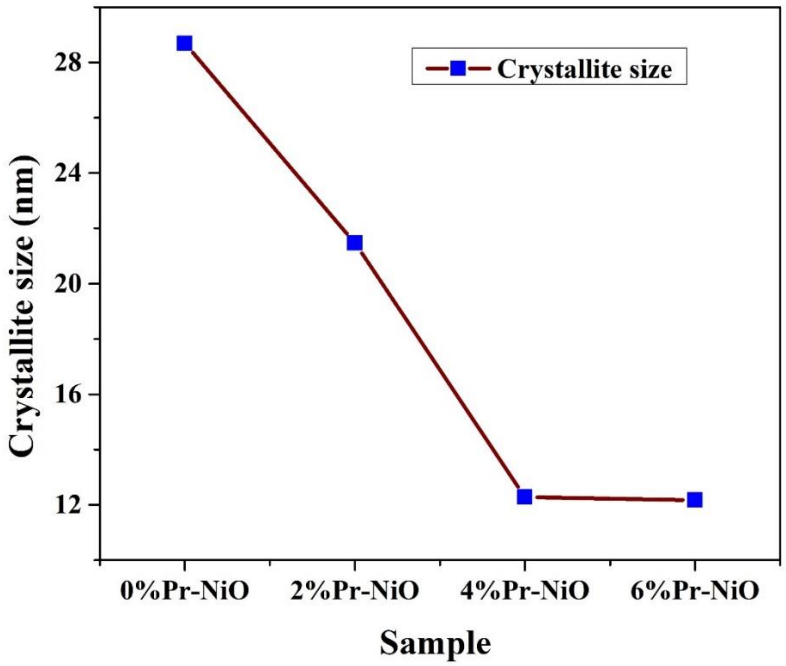


Figure 4-2 Crystallite size of the graph of NiOx and Pr-doped NiOx thin films

## 4.2 Morphological Analysis

This analysis is important due to several factors. As the morphology and topography in the thin-films industry play an imperative role in the properties and the usage in the industrial sector, it needs to be carefully studied. To study the morphology SEM was utilized whereas to study the topography and roughness parameters AFM was employed.

### 4.2.1 Analysis of scanning Electron microscope (SEM)

For the morphological analysis of synthesized thin films, SEM (JEOL Number) with an accelerated voltage of 20 kV was used, samples were spin-coated onto the FTO glass substrate and micrograph of undoped and Pr-doped $NiO_x$ thin film are shown in the Fig 4.3. It can be seen that in Fig 4.3 (a-c) thin film with uniform smooth compact and pinhole free coverage on FTO glass substrate which could reduce the charge recombination and increased open-circuit voltage. In Fig 4.3 (d) SEM micrograph shows 6%Pr-doped $NiO_x$ found pinhole on thin film.

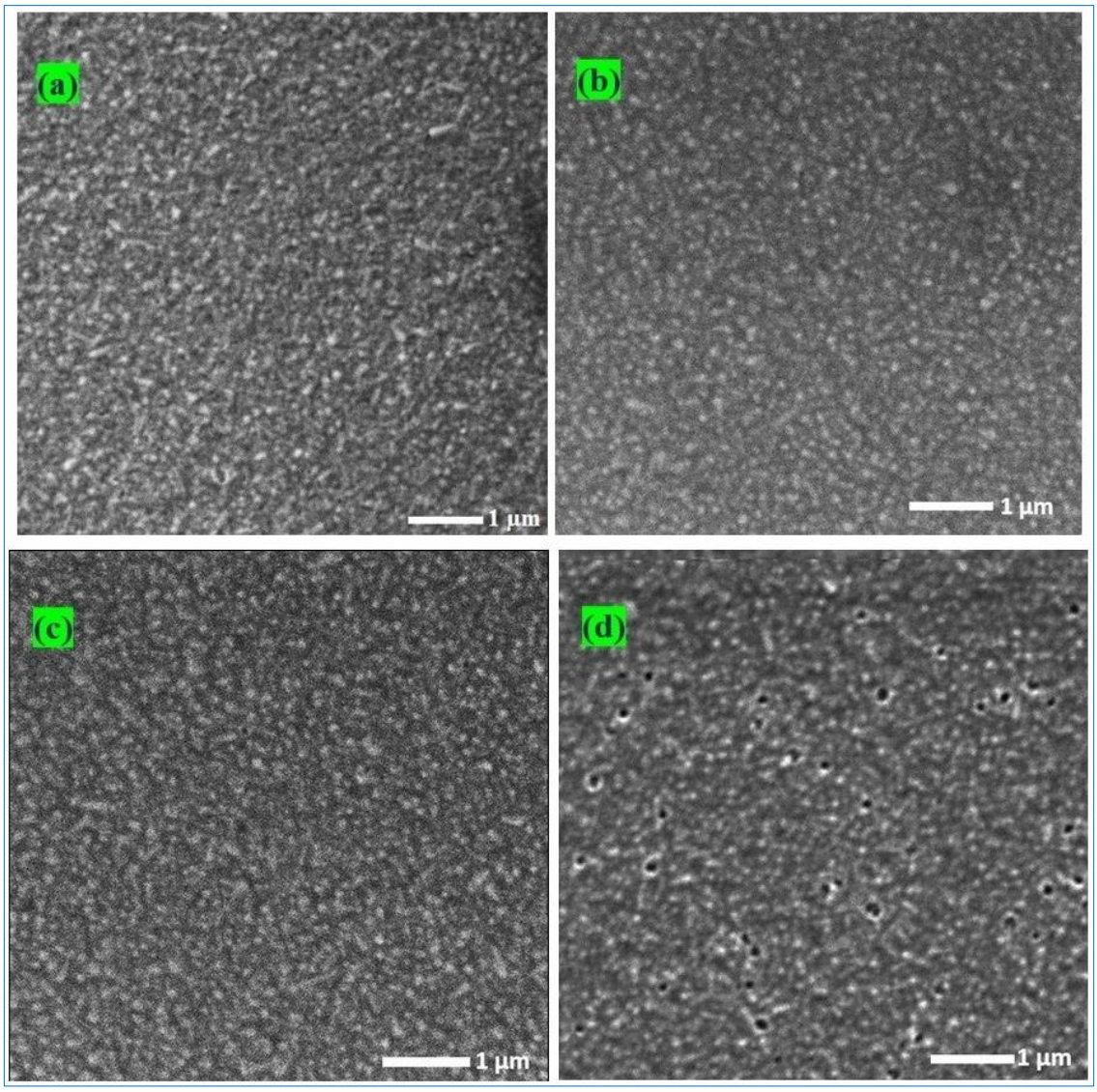


Figure 4-3 SEM result for undoped and Pr-doped NiOx

### 4.2.2 Energy Dispersive spectroscopy (EDS)

Fig 4.4 to 4.7 shows the EDS results of undoped and Pr-doped $NiO_x$ thin films, showing the presence of the Ni, O, and Pr peaks were observed in different detection points in the thin film samples, no impurities can be detected. The tin (Sn) peaks seem to be originated from the FTO glass substrate. These results are consistent with our XRD result. These results are summarized in Table 4.4(a), 4.5(b), 4.6(c) and 4.7(d) are shown Ni, O, and Pr elements have different weights and atomic percentages.

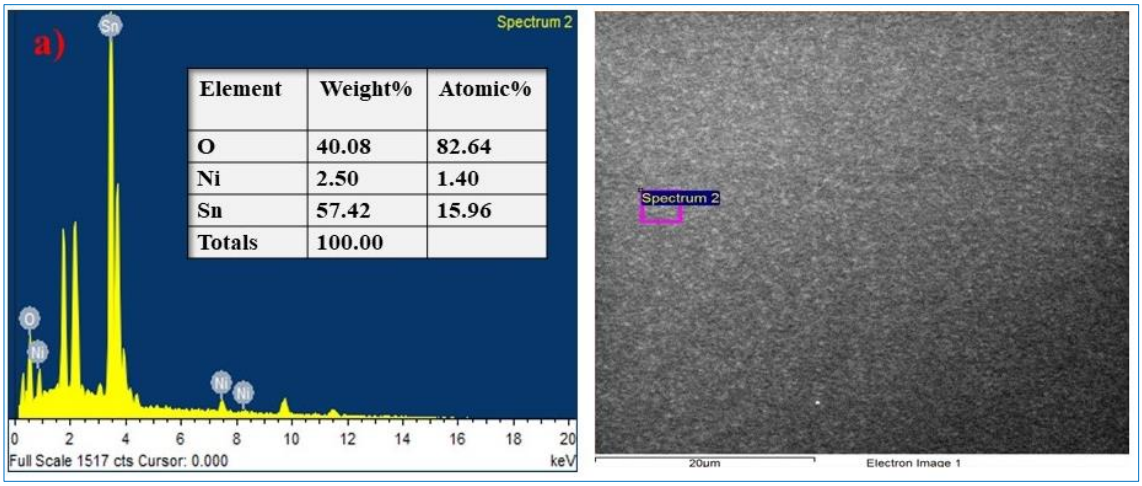


Figure 4-4 (a) EDS pattern of 0%Pr-doped NiOx

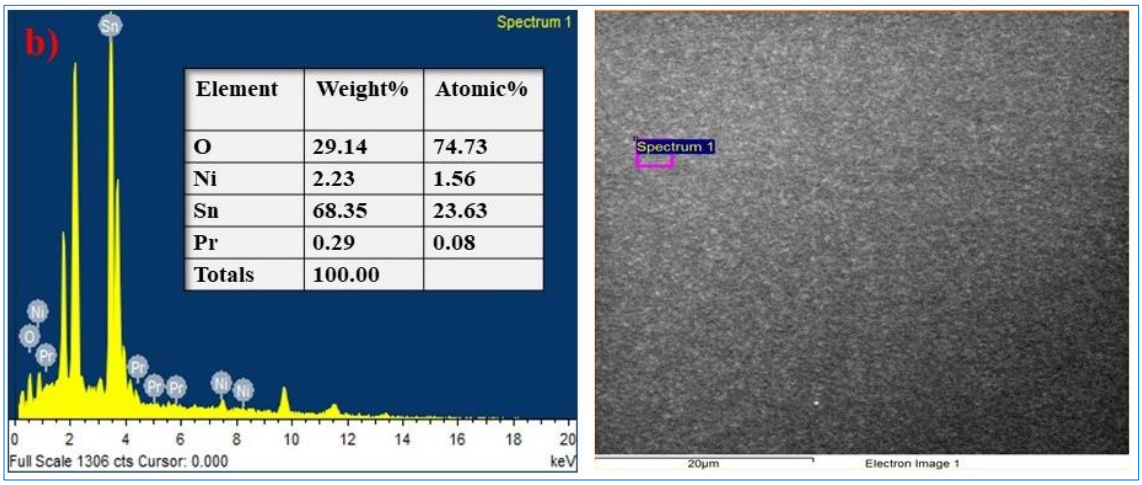


Figure 4-5 (b)  EDS pattern of 2%Pr-doped NiOx

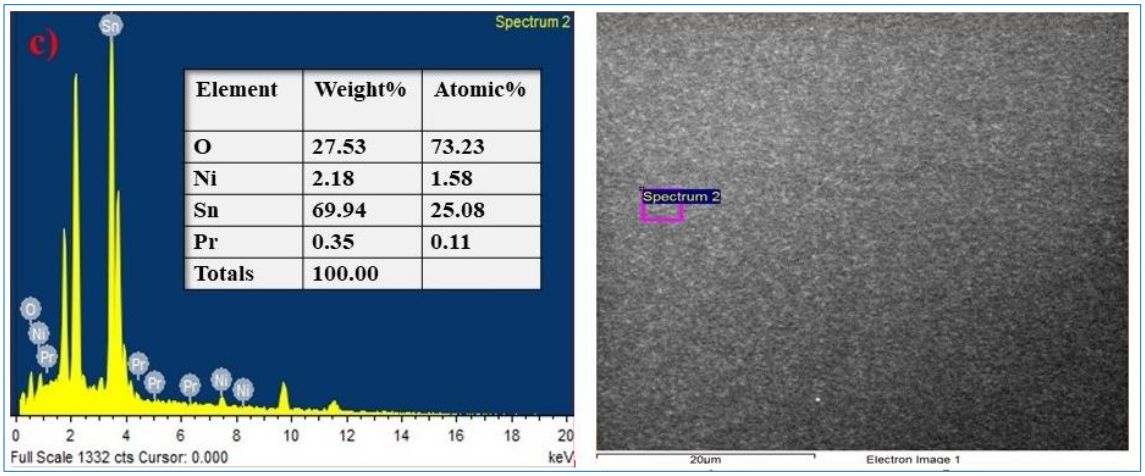


Figure 4-6 (c) EDS pattern of 4%Pr-doped NiOx

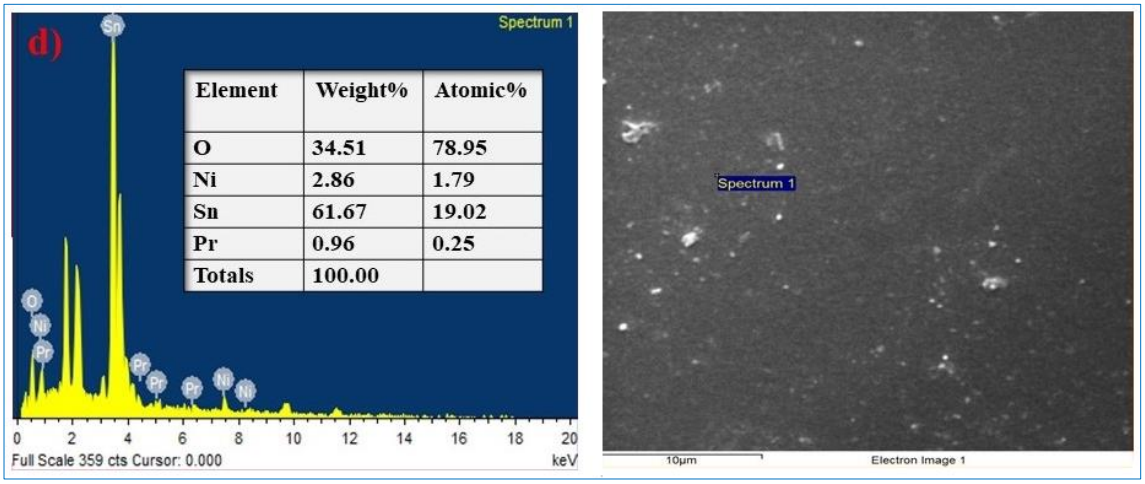


Figure 4-7 (d) EDS pattern of 6%Pr-doped NiOx

### 4.2.3 Analysis of Atomic force microscopy

For further investigation about thin-film structure, surface roughness, and morphology of undoped and Pr-doped $NiO_x$ film, the prepared films were characterized by using 3-Dimensional AFM as depicted in Fig 4.8. This shows that undoped $NiO_x$ and 2, 4, and 6 mol% Pr-doped $NiO_x$ thin film as shown in the Fig 4.8 (b), Fig 4.8 (c), Fig 4.8 (d), and Fig 4.8(e) respectively, no agglomeration is present, and pinhole-free thin is obtained. Furthermore, the AFM micrograph confirmed that the uniform and crack-free morphologies of pristine and Pr-doped $NiO_x$ thin film. it should be noted here that flat and uniform and the surface of HTL is beneficial to the formation of higher quality perovskite film with large scale uniformity. This could also reveal that the Pr-doped $NiO_x$ thin film may be beneficial for HTL in perovskite solar cells. The results, we find are fully consistent with previous results [3, 4].

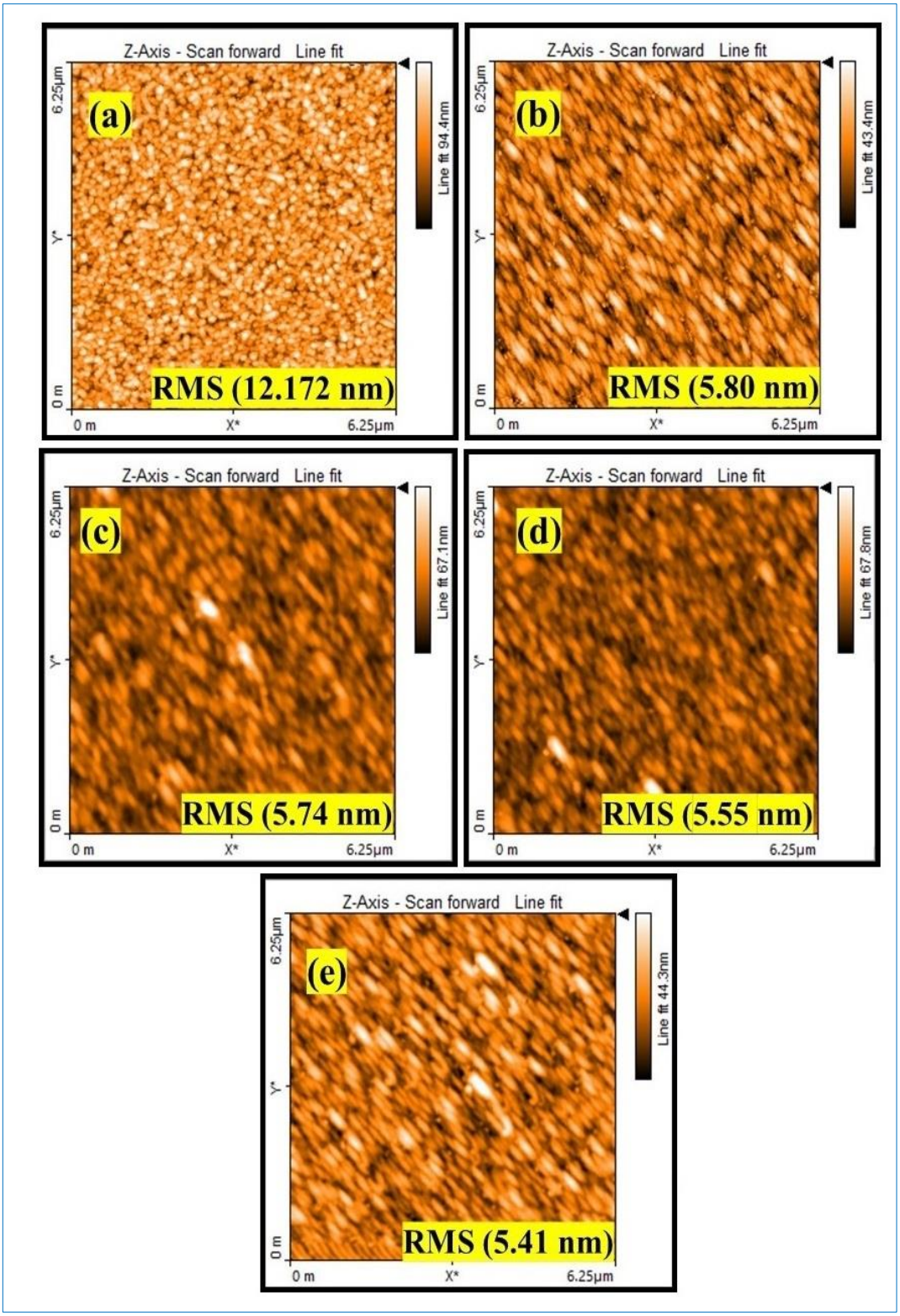


Figure 4-8 AFM result of undoped and Pr-doped NiOx thin films

Moreover, the surface Root mean square (RMS) values of undoped and Pr-doped $NiO_x$ concentrations 2, 4, and 6 mol% thin films have been calculated and shown in Fig 4.9 respectively, and calculated values are summarized in Table 4.2. The roughness of blank FTO is 12.172 nm in Fig 4.8 and the doped samples have shown a continuous decline roughness parameter associated with rising concentration in mol%. This showed a planer surface than that of undoped $NiO_x$. It was considered that the planer surface of the charge carrier transport layer could cause a good power contact with the perovskite solar absorber layer.

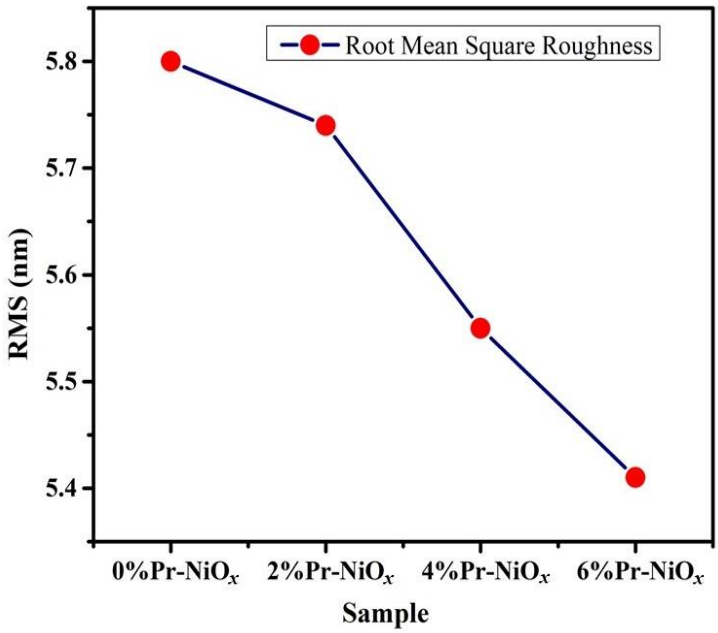


Figure 4-9 Root mean square roughness of NiOx and Pr-doped NiOx

Table 4-2 Root mean square roughness NiOx and Pr-doped NiOx

| S.No | Samples | Root Mean Square Roughness (nm) |
|---|---|---|
| 01 | 0%Pr-$NiO_x$ | 5.80 |
| 02 | 2%Pr-$NiO_x$ | 5.74 |
| 03 | 4%Pr-$NiO_x$ | 5.55 |
| 04 | 6%Pr-$NiO_x$ | 5.41 |

## 4.3 Optical Measurements of thin films

Optical measurements are important for several reasons such as finding out different sample properties and their behavior in the visible light spectra which is vital for the ETMs. This is also important to study the optical behavior of Ag incorporation into the $TiO_2$ matrix and how optical properties are affected. The following are the characterization measurements taken.

### 4.3.1 Ultraviolet-visible spectroscopy (UV-VIS) of thin films

UV-visible spectroscopy yields a spectrum of absorption and transmittance of light which provides knowledge about the amount of light passing through various wavelengths are depicted in Fig 4.10(a and b). The optical transmittance of pure $NiO_x$ and Pr-doped $NiO_x$ thin film coated on a glass slide. Undoped $NiO_x$ and 2% Pr-doped $NiO_x$ show high transmittance nearly about 85% in the visible range between 400 nm to 750 nm. But when $NiO_x$ are doped 4% and 6% with Pr-ions then optical transparency is gradually declined with increasing concentration of Pr content. Moreover, the optical transparency of thin-film is based on various other prospects also as instance film roughness, size of the grain, thickness, and discrepancy in processing, etc. Thin-film transparency could be changed by the impact of these elements. our results are consistent with previous studies [5].

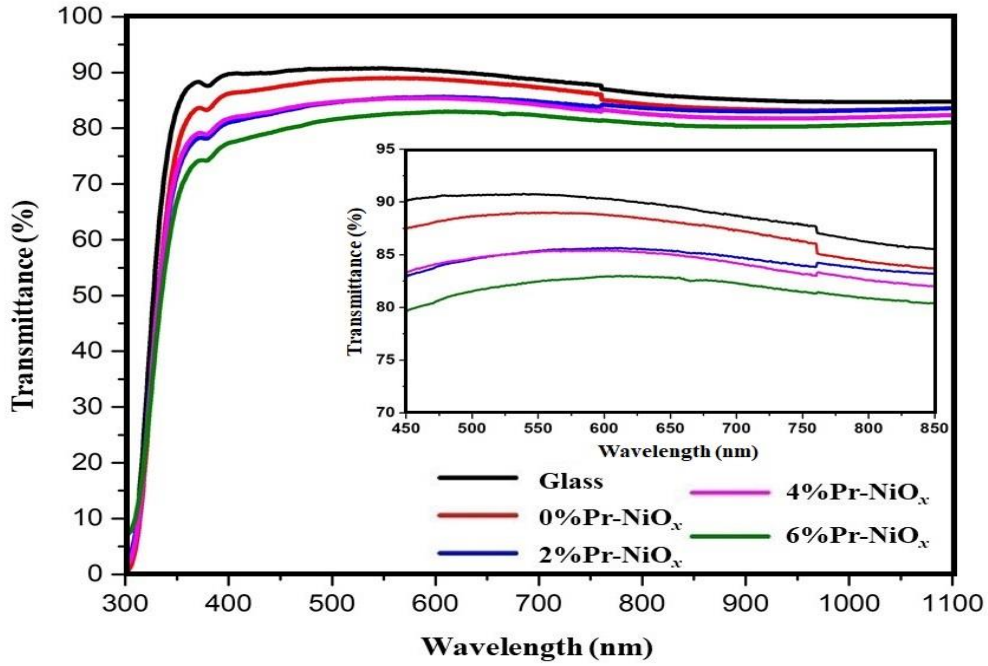


Figure 4-10 (a) UV-vis Transmittance spectra of undoped 0%Pr-NiOx, 2%Pr-NiOx, 4%Pr-NiOx, and 6%Pr-NiOx, inset enlarge spectra in the 450 nm to 850 nm range.

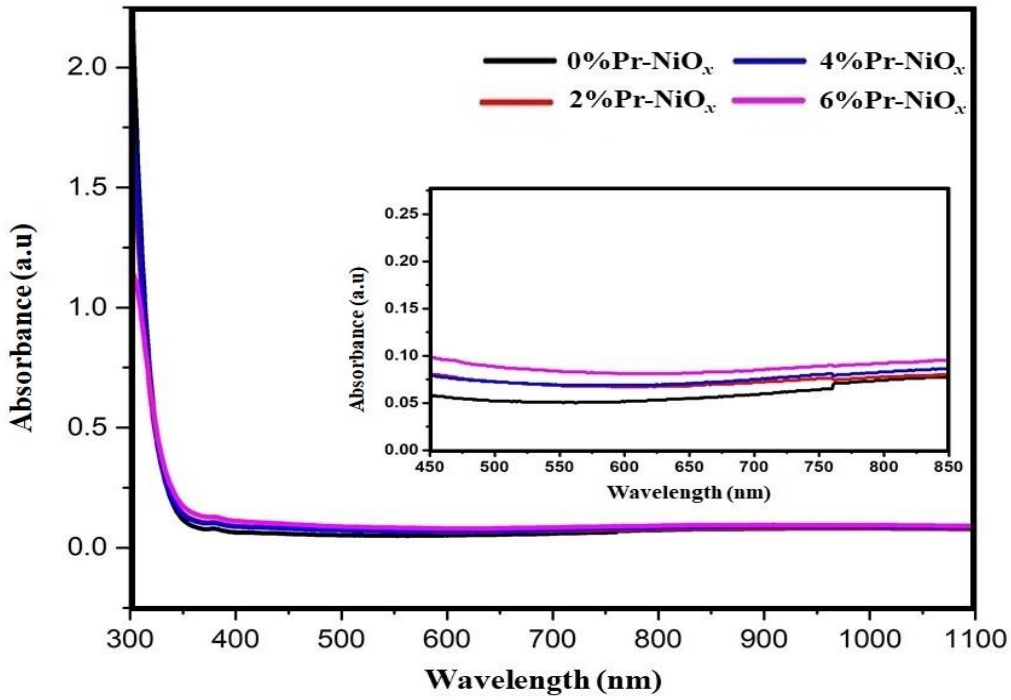


Figure 4-10 (b) Absorption spectra of 0%Pr-NiOx, 2%Pr-NiOx, 4%Pr-NiOx, and 6%Pr-NiOx and inset enlarge absorption spectra in the 450 nm to 850 nm range.

The film thickness of the Pr-doped $NiO_x$ is determined to be approximately 34 nm from the optical profilometry. The optical band gap ($E_g$) of thin films was acquired from the absorption data applying Tauc's equation [6].

Where $\alpha$ shows the Absorption coefficient of the film, $h\upsilon$ is the energy of the photon, $B$ is a constant and $E_g$ represents optical bandgap. $E_g$ has been obtained by extrapolating the rectilinear region of $(\alpha h\upsilon)^2$ vs photon energy $(h\upsilon)$ on the energy axis as revealed in Fig 4.11 and Fig 4.12. The optical band gap value of undoped $NiO_x$ is 3.91ev which is well-matched with the reported band gap value for undoped $NiO_x$ thin film. It can be observed that optical band gap values were slightly get decreased from 3.91 eV to 3.76 eV as depicted in Fig 4.11 (a, b) and 4.12 (c, d) with enhancing the concentration of Pr content (0 to 6 mol%). Reduction in bandgap has also been reported in Li doped $NiO_x$ thin film via sol-gel technique [7].

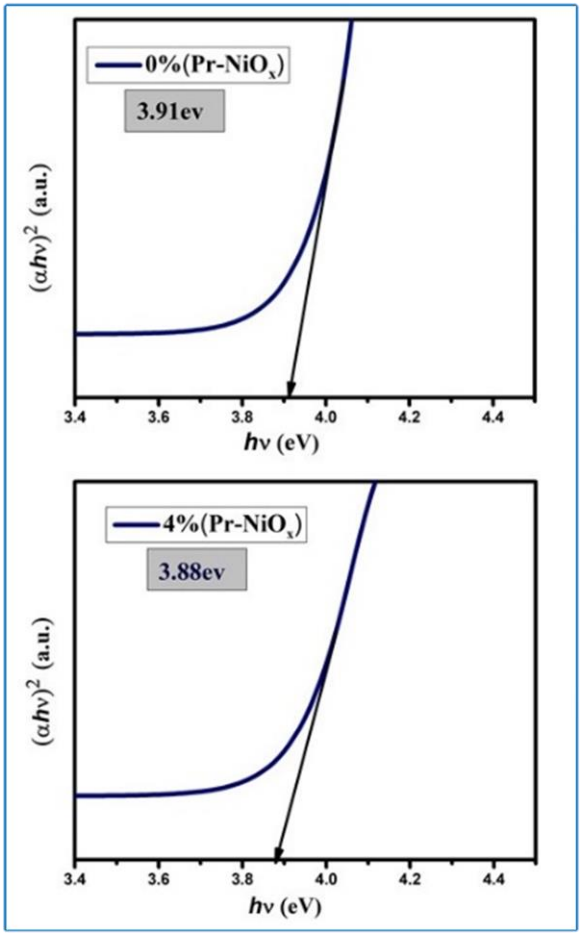


Figure 4-11 Optical band gap of (a) undoped 0%Pr-NiOx (b) 4%Pr-NiOx

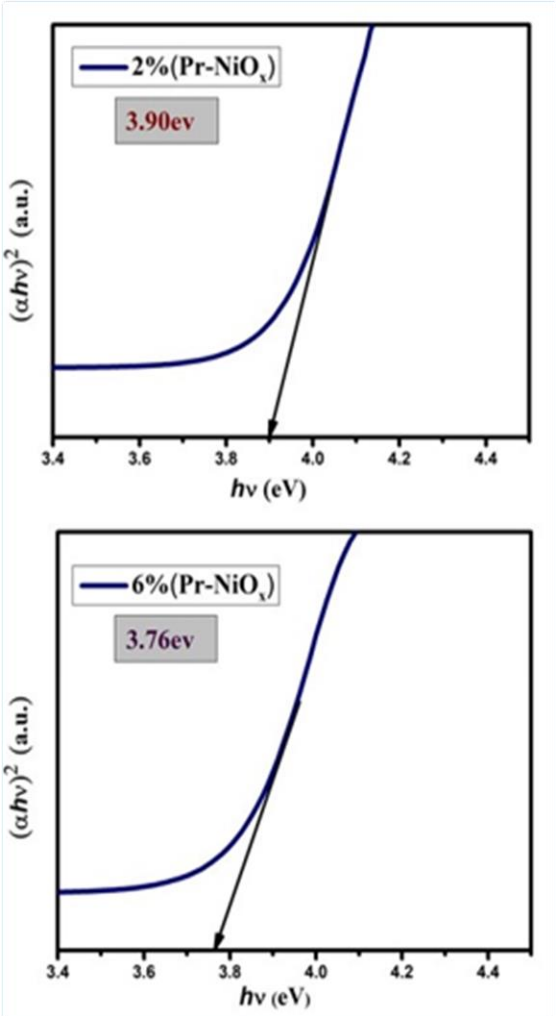


Figure 4-12 Optical band gap of (a) 2%Pr-NiOx (b) 6%Pr-NiOx

**4.4 Hydrophobicity Measurement**

The wettability of the solid surface is measured by the contact angle. The contact angle of water droplets was initially calculated by Thomas young who modeled the static contact angle of a droplet on a smooth surface, super-hydrophilic or super-wetting surface has contact angle less than 30° [8], and it can also be used to determine the hydrophobic nature of the solid surface and surface tension component. Fig 4.13(a and b) indicates snapshots of the goniometry when a 5 µm drop of liquid is placed on a fabricated dry thin film of $NiO_x$ and Pr-doped $NiO_x$ surface of the glass substrate to observe the contact angle. The contact angle of a $NiO_x$ and Pr-doped $NiO_x$ thin film is 12.10° and 9.20° which shows the abruptly raised hydrophilicity of the Pr-doped $NiO_x$ thin film. As a result, enhanced the wettability of Pr-doped $NiO_x$ thin film link with higher interfacial interaction among

Pr-doped $NiO_x$ and an active layer of perovskite, facilitating the arrangement of a homogenous better quality of perovskite thin film. in general, the surfaces generating an angle more than 90° are of hydrophobic but with keeping view the viscosity of water, any angle closer to 90° is highly hydrophobic [9].

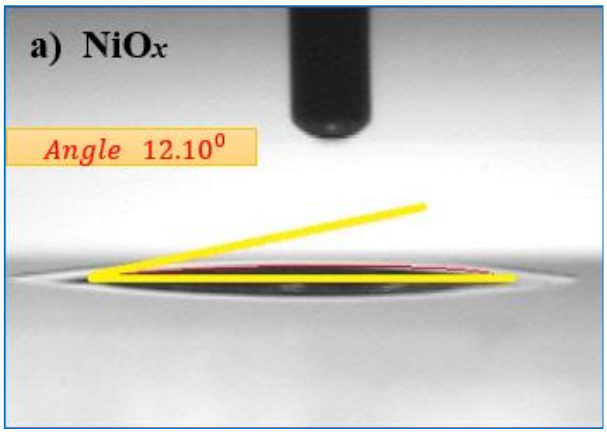


Figure 4-13 (a) Contact Angle Measurement of NiOx on FTO Glass substrate

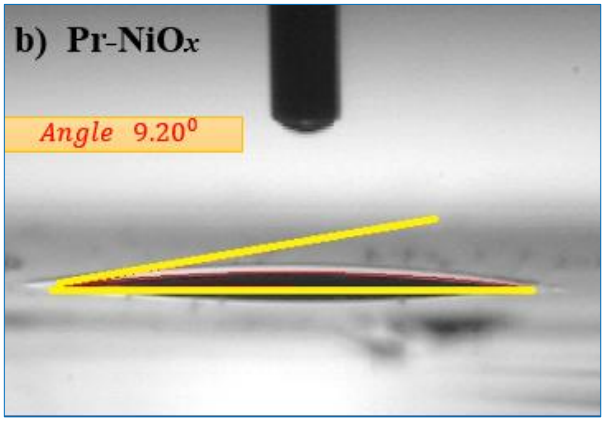


Figure 4-13 (b) Contact Angle Measurement of Pr-doped NiOx on FTO Glass substrate

## 4.5 Electrical properties analysis

Electrical analyses were carried out for the thin film to study the generation of electron and hole pairs with the interaction of material and with light and effect that has been produced due to Pr doping in the $NiO_x$ lattice structure. These were vital for the application-dependent properties of ETMs such as mobility and conductivity. The subsequent are the electrical characterization carried out for our samples.

### 4.5.1 DC-Hall effect measurement

DC-Hall effect system was used to measure the resistivity, conductivity. Hence, a swin system of 5300G magnetic field was employed in the Hall effect system whilst measurements were taken under dark conditions and at a temperature of 300 K. The hall effect system utilizes four probes the method which is essential for the accurate measurements of the thin film properties.

The result is shown in Fig 4.14(a and b) and summarized in Table 4.3, show conductivity and resistivity respectively. Here the undoped $NiO_x$ gives low conductivity which is 4.68 $x10^{-6}$ S $cm^{-1}$ and the pure $NiO_x$ gives high resistivity which is 2.18 $x10^5$ Ω-cm it is mentioned here that incorporation of Pr-ions can significantly enhance the electrical conductivity of un-doped $NiO_x$ thin film as compared with 4% Pr- $NiO_x$ thin film layer. Conductivity increases with Pr-doped concentration in case of (2 and 4% Pr doped $NiO_x$) were measured to be 7.65 $x10^{-6}$ S $cm^{-1}$ and 8.27 $x10^{-6}$ S $cm^{-1}$ respectively, probably because of enhanced the carrier concentration [10].

Table 4-3 Conductivity and resistivity of undoped NiOx and different concentrations of Pr-doped NiOx thin films.

| S.No | Conductivity [S $cm^{-1}$] | Resistivity [Ω-cm] |
|---|---|---|
| 01 | 4.68 x $10^{-6}$ | 2.18 x $10^5$ |
| 02 | 7.65 x $10^{-6}$ | 1.32x $10^5$ |
| 03 | 8.27 x $10^{-6}$ | 1.22x $10^5$ |
| 04 | 5.97 x $10^{-6}$ | 1.69x $10^5$ |

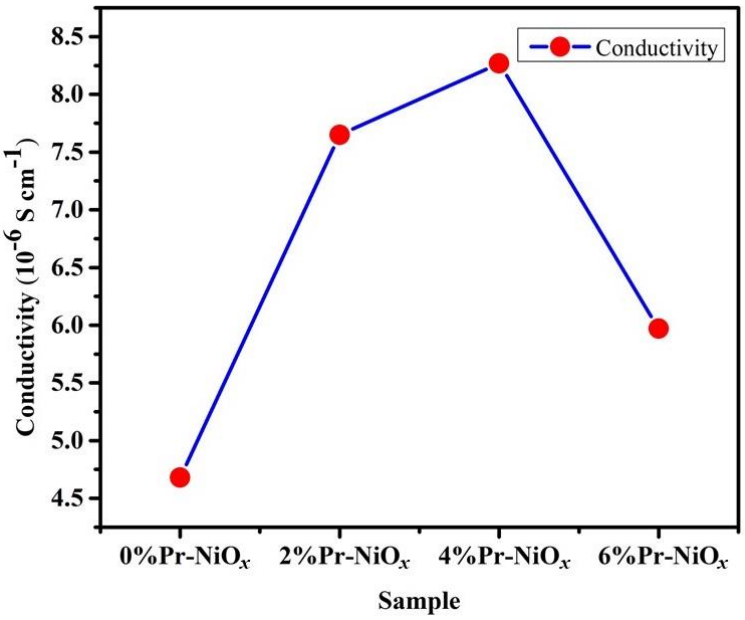


Figure 4-14 (a) Conductivity graph for NiOx and Pr-doped NiOx thin films

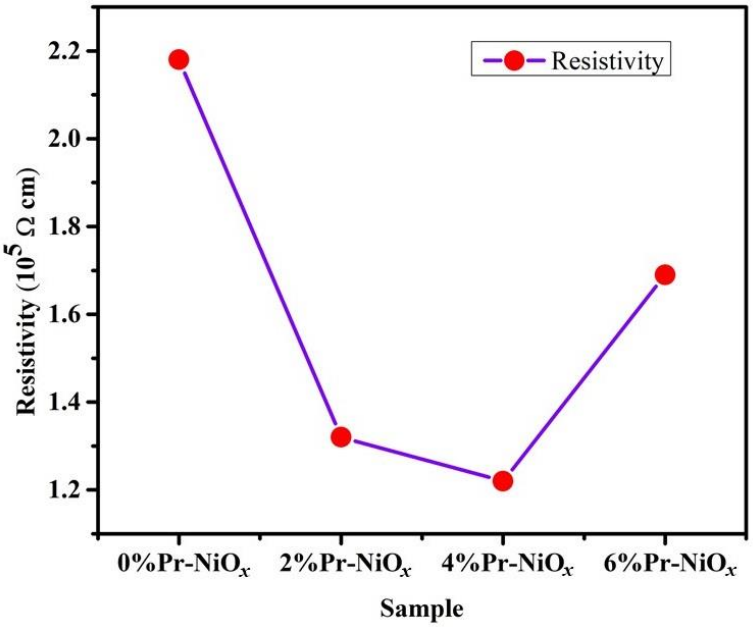


Figure 4-14 (b) Resistivity graph for NiOx and Pr-doped NiOx thin films

### 4.5.2 IV Curve measurement

The I-V curve is a graph of all possible available combinations of voltage and current operated under constant conditions and gives the characteristic electrical properties of a solar cell depending upon the active electrode region that enhances charge transport, exciton dissociation, and carrier injection. These properties a usually measured using a Keithley source meter under illuminated and dark conditions. Generally, the I-V curve has a characteristic shape point, the behavior is similar however when it is to the right of the MPP, there is an immediate decline in power output because of sealed charges within the solar cell that do not flow out. These charges are a result of increased voltage output. IV-curve gives the $J_{sc}$, $V_{oc}$, and Fill Factor FF for the device under consideration and this information can be used to find the efficiency of the cell. I-V characteristics of the cells are shown as in Fig 5.18 and corresponding photovoltaic device parameters are listed in the Table 4.4 such as $V_{oc}$, $J_{sc}$, FF, and PCE. It is evident from the Fig 4.15 that using Pr-doped $NiO_x$ as HTL in PSC affected the $V_{oc}$ and $J_{sc}$ value. The PCE of the Pr-doped $NiO_x$ HTL based PSC was enhanced at first and then dropped in comparison to the undoped $NiO_x$ HTL based PSC, upon employing 2%Pr-doped $NiO_x$ HTL PSC revealed a PCE of 9.10% with an enhanced of 31.69%. the performance of the device is remarkably improved when employing 4% Pr-doped $NiO_x$ HTL based PSC has shown that 9.23% PCE, resulting in 33.57% better improvement in PCE as compared to a device utilizing undoped $NiO_x$ based HTL. When doping concentration of Pr-ions is increased further up to 6 mol%, photons to electron conversion efficiency dropped down to 9.0%, the lower performance of PCE in this device significantly greater doping level could be due to increased charge carrier recombination, longer carrier lifetime, and lowered electrical conductivity carry adverse impact on the performance of the device.

Table 4-4 Photovoltaic Device parameters of HTLs based PSCs NiOx and Pr-doped NiOx

| HTLs | Voc (v) | Jsc (mA $cm^{-2}$) | FF (%) | PCE (%) |
|---|---|---|---|---|
| 0% Pr-$NiO_x$ | 0.85 | 12.273 | 66.3 | 6.91 |
| 2% Pr-$NiO_x$ | 0.95 | 12.922 | 74.2 | 9.10 |
| 4% Pr-$NiO_x$ | 0.99 | 17.147 | 54.4 | 9.23 |
| 6% Pr-$NiO_x$ | 0.98 | 16.000 | 57.4 | 9.00 |

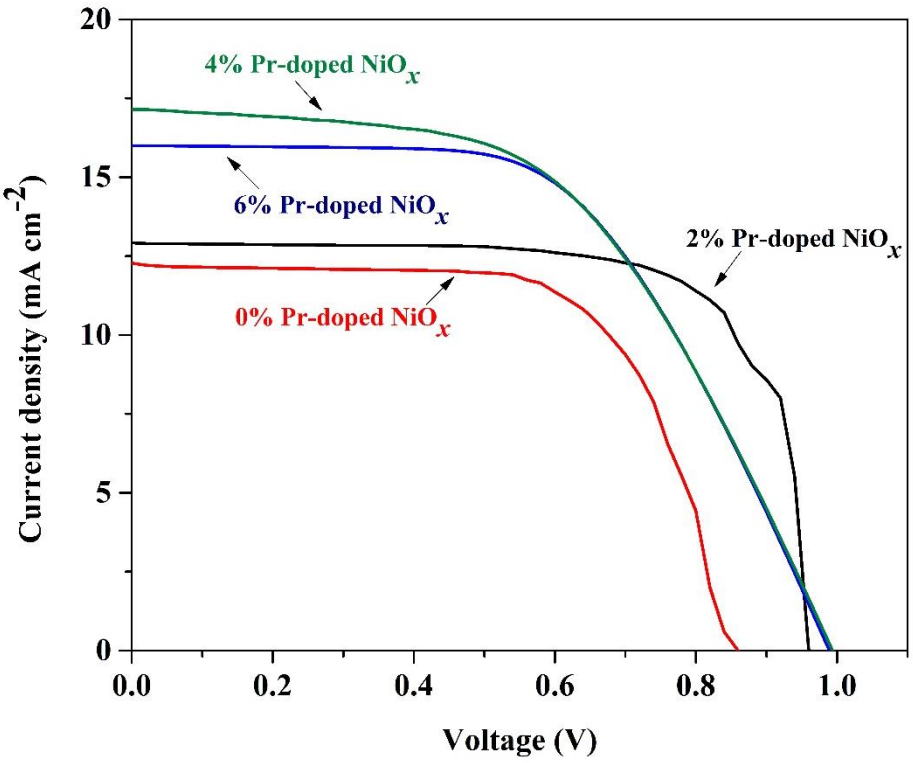


Figure 4-15 J-V characteristic curves of undoped and Pr-doped NiOx PSC

## References


1. Shannon, R.D., Revised effective ionic radii and systematic studies of interatomic distances in halides and chalcogenides. Acta Crystallographica Section A, 1976. **32**(5): p. 751-767.
2. Hu, Z., et al., Sol-gel-processed yttrium-doped NiO as hole transport layer in inverted perovskite solar cells for enhanced performance. 2018. **441**: p. 258-264.
3. Kotta, A. and H.K. Seo, Facile Synthesis of Highly Conductive Vanadium-Doped NiO Film for Transparent Conductive Oxide. Applied Sciences, 2020. **10**(16).
4. Zheng, J., et al., Solution-Processed, Silver-Doped NiOx as Hole Transporting Layer for High-Efficiency Inverted Perovskite Solar Cells. ACS Applied Energy Materials, 2018. **1**(2): p. 561-570.
5. El Radaf, I., H. Al-Zahrani, and A.S. Hassanien, Novel synthesis, structural, linear and nonlinear optical properties of p-type kesterite nanosized Cu2MnGeS4 thin films. Journal of Materials Science: Materials in Electronics, 2020. **31**.
6. Sawaby, A., et al., Structure, optical and electrochromic properties of NiO thin films. Physica B: Condensed Matter, 2010. **405**: p. 3412-3420.
7. J, A. and T. Sahoo, Effect of Li doping on conductivity and band gap of nickel oxide thin film deposited by spin coating technique. Materials Research Express, 2019. **7**(1): p. 016405.
8. Haider, A.J., et al., Enhance Preparation and Characterization of Nickel-Oxide as Self-Cleaning Surfaces. Energy Procedia, 2019. **157**: p. 1328-1342.
9. Zhou, W., et al., Successive surface engineering of TiO2 compact layers via dual modification of fullerene derivatives affording hysteresis-suppressed high-performance perovskite solar cells. Journal of Materials Chemistry A, 2017. **5**(4): p. 1724-1733.
10. Zhou, H., et al., Photovoltaics. Interface engineering of highly efficient perovskite solar cells. Science, 2014. **345**(6196): p. 542-6.

# Chapter 5: Conclusions & Future Recommendation

## Conclusions

P-type $NiO_x$ and Pr-doped $NiO_x$ thin film thickness approximately (35nm) was measured by optical profilometry and fabricated on FTO glass substrate using the sol-gel spin-coated method. Moreover, the doping concentration of Pr-ions varies from 2 mol% to 6 mol%. The fabricated p-type $NiO_x$ and Pr-doped $NiO_x$ thin film were characterized by XRD, SEM/EDX, AFM, Hall effect, UV-vis spectrometry, and I-V measurement system. the interrelation between varying doping concentration and their prepared surface morphology, structural, optical, and photovoltaic properties were examined and elucidated. Cubical structural of $NiO_x$ have revealed by XRD results with having highest intensity peak at (2 0 0) crystal plane. The crystallite size of the prepared thin film decreases with increasing doping concertation from 28 nm to 12 nm. The AFM micrograph results show the surface roughness of thin film which decreases from 5.80 nm to 5.41 with increasing the doping concentration SEM micrograph results shows the smooth, uniform, compact, and coverage on FTO glass substrate. EDS results shows the peaks of Ni, O, and Pr element and no impurities can be detected. Thin films were transparent in ( 450 nm to 850 nm) visible region and their transmittance decreased with increasing the doping concentration. UV-vis transmission spectra were used to calculate bandgap which decreases from 3.91 eV to 3.76 eV with enhanced Pr doping concentration. Hall effect measurement shows the conductivity and resistivity of thin-film, conductivity is increased, and resistivity decreases with increasing the doping concentration. It was noted that the cell fabricated by employing 4%Pr-doped $NiO_x$ HTL based PSC exhibited the better performance of Voc and FF than that undoped $NiO_x$ HTL based PSC.

## Future Recommendations

It would be fascinating to learn more about what causes perovskite solar cells to degrade under steady illumination in order to find a solution to prevent this. Because it is currently

the most significant impediment to their commercialization. Alternative materials for each layer (HTL, absorbing layer, ETL) of the PSC structure might also be interesting to study, to investigate whether other materials can help to improve the cell and prevent deterioration. There is also a further need to increase the efficiency and minimize the production cost of inverted planar structure (p-i-n) PSC.

# Appendix A- Publication

## Praseodymium Doped Nickel Oxide as Hole-Transport Layer for Efficient Planar Perovskite Solar Cells

*Muhammad Tahir[a], Hafiz Muhammad Abd-ur Rehman[b], Asif Hussain Khoja[a], Mustafa Anwar[a], Adil Mansoor[c], Faisal Abbas[a], Sehar Shakir[a,*]*

*[a]U.S-Pakistan Center for Advanced Studies in Energy (USPCAS-E), National University of Sciences & Technology (NUST), H-12 Campus, Islamabad, Pakistan*
*[b]School of Mechanical & Manufacturing Engineering (SMME), National University of Sciences & Technology (NUST), H-12 Campus, Islamabad, Pakistan.*
*[c]Department of Chemistry, School of Natural Sciences, National University of Sciences and Technology, (NUST) H-12 Campus, Islamabad, Pakistan.*

**Abstract**

Hybrid organic/inorganic Perovskite Solar Cells (PSCs) have acquired significant consideration due to high power conversion efficiency (PCE). In PSCs, electron and hole extraction layers have a significant influence on their overall performance. In inverted p-i-n structure-based PSCs, $NiO_x$ has been frequently employed as a Hole Transport Layer (HTL) due to its simple processing, wide bandgap, high optical transmittance, excellent chemical stability, and low processing temperature for large scale fabrication. However, $NiO_x$ suffers from low electrical conductivity. Doping of $NiO_x$ is an effective technique employed for enhancing electrical as well as optical properties. Herein, for the first time, Praseodymium doped $NiO_x$ (Pr-$NiO_x$) was synthesized by sol-gel method, and films were fabricated to investigate the effect of Pr dopant on the optoelectronic properties and photovoltaic performance of PSCs. Results indicated that Pr doping significantly improved conductivity of $NiO_x$ films from 4.68 x $10^{-6}$ S $cm^{-1}$ to 8.27 x $10^{-6}$ S $cm^{-1}$. Moreover, it also enhanced the compactness, and interfaces of $NiO_x$ HTL. PSCs based on 4% Pr-doped $NiO_x$ HTL- yielded PCE of 9.23% which is 33.57% more than the PSCs fabricated using undoped $NiO_x$ HTL. The enhanced PCE of PSC devices with Pr-doped $NiO_x$ could be attributed to efficient extraction of a hole from an active absorbing layer

of perovskite thereby, lowering the probability of unsuitable charge carrier recombination. This work exhibit that Pr-doped $NiO_x$ thin film could be a promising alternative material for efficient and stable inverted PSCs.

**Keywords:** *inverted planar perovskite solar cell; Pr-doped $NiO_x$; Sol-gel Process; hole transport layer; Thin film;*

Journal: Journal of Alloys and Compounds

Current Status: Under Review

Date: March 09, 2022